On the assessment of pedestrian distress in urban winds

Vita, Giulio; Shu, Zhenru; Jesson, Mike; Quinn, Andrew; Hemida, Hassan; Sterling, Mark; Baker, Christopher

On the assessment of pedestrian distress in urban winds

Giulio Vita, Zhenru Shu, Mike Jesson, Andrew Quinn,
Hassan Hemida, Mark Sterling , Chris Baker

Department of Civil Engineering, University of Birmingham, Edgbaston, Birmingham, UK

Abstract:

Urban winds can cause a risk to pedestrian safety if not properly assessed. High-rise buildings produce a complex flow field at ground level, where regions of accelerated and recirculating flows are present. Gust wind speeds provide an indication of the maximal speed pedestrian might experience due to the unsteady flow. In this study, low- and high-fidelity numerical and experimental techniques to predict pedestrian level winds are tested on a realistic full-scale test-route at the University of Birmingham Campus during a storm event. Results show that it is beneficial to increase the complexity of simulations as a direct correspondence exists between the gust wind speed and the turbulent environment. While not much gain is achieved switching from Irwin Probes to hot-wire anemometry, LES greatly outperforms RANS and challenges experimental simulations in terms of reliability. The validity of the peak factor is also questioned and a general comment on the adequacy of each technique is discussed.

Keywords: urban flow, large eddy simulation, wind tunnel, pedestrian wind, gustiness.

1 Introduction

In the urban planning of new developments, it has become normal practice to evaluate the wind microclimate in order to guarantee the comfort and safety of pedestrians (Cammelli and Stanfield, 2017), particularly around tall buildings. Concerns over pedestrian safety in the UK have recently increased following an accident that occurred in March 2011 in the city of Leeds. The inaccurate assessment of wind conditions near Bridgewater Place (the tallest building in the city) caused the overturning of a lorry, killing one pedestrian and injuring another (BBC, 2017). This has caused the need to design and place a complex wind mitigation system at the base of the building (BBC News, 2014), costing the owners ~£900,000 of unpremeditated expense (BBC News, 2016). New developments must now comply to Wind Microclimate Guidelines, which in the UK are being implemented in London (City of London Corporation, 2019) and Leeds (Leeds City Council, 2019).

As the risk of pedestrians due to the wind environment around tall buildings is present and real, wind mitigation systems, such as shelters, much be planned and designed to tackle risk by reducing the wind speed. A risk based methodology has been recently proposed to overcome the limitations in current design practice of designing

wind mitigation systems based on wind speed magnitudes and probability of exceedance only, where the effect on pedestrians is only evaluated indirectly through wind distress criteria (Baker, 2015). Figure 1 shows a flow chart for the design of the wind environment around tall buildings based on a risk analysis, taking into account not only the probability of a wind speed to be exceeded but also how pedestrians respond, their activity and the related consequences of an accident.

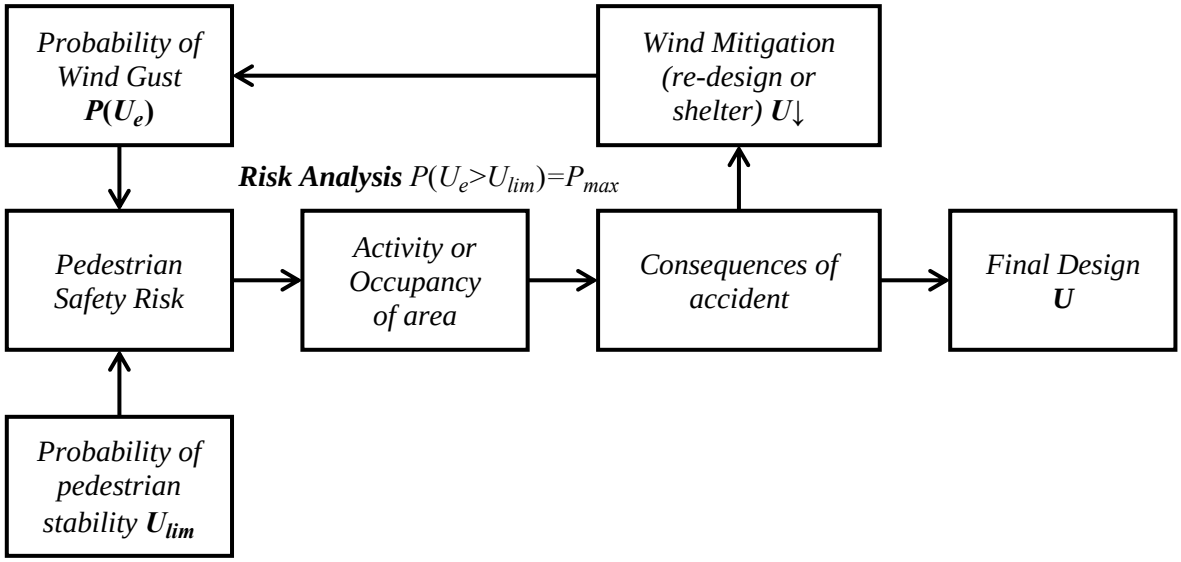

Figure 1. Pedestrian safety and wind environment around buildings risk flow chart (adapted from Baker, 2015)

Pedestrian distress criteria are usually defined with an expression of the type

$$U_e > U_{lim} \quad (1);$$

where U_e is an effective wind speed and U_{lim} an appropriately defined distress threshold (Lawson and Penwarden, 1976). A suitable exceedance probability P_{max} is defined so that the safety criterion yields (Blocken and Carmeliet, 2004; Bottema, 2000)

$$P\,(U_e > U_{lim}) = P_{max} \quad (2);$$

U_e and U_{lim} are based on either the mean wind speed U or the gust wind speed U_g (Hunt et al., 1976). U_e is computed by assessing the wind speed probability distribution of the wind environment at the base of buildings through numerical and/or experimental simulation (Blocken et al., 2016). Results are then compared to a distress threshold U_{lim} using a safety criterion of choice. This distress threshold may vary due to a number of factors.

- The age of pedestrians, with lower distress values for elderly (Bottema et al., 1992);
- The activity of pedestrians (Lawson and Penwarden, 1976; Penwarden et al., 1978; Soligo et al., 1998);
- The typology of wind: uniform, non-uniform or gust (Hunt et al., 1976);
- The duration of gusts (Melbourne, 1978; Peters, 1999).

Table 1 gives an overview of pedestrian safety criteria as found in literature (adapted from Jordan *et al.*, 2008).

It can be seen that the threshold values vary significantly, which suggests more research is needed to specify the distress condition. (Baker, 2015; Blocken et al., 2016; Jordan et al., 2008; Stathopoulos, 2006).

Table 1 Summary of critical wind speeds for human stability (*adapted from* Jordan *et al.*, 2008)

Reference	*Distress Threshold Wind Speed U_{lim}* (m/s)		*Exceedance Probability P_{max}* (%)	*Notes*
	Gust Wind Speed U_g	*Mean Wind Speed U*		
British Railways Board, 1970	*11-17*	-	-	*From Japanese Railway Criteria personnel and passengers*
Isyumov and Davenport, 1976	-	*15.22*	*0.02* %	-
Hunt, Poulton and Mumford, 1976	*20*	*13–15*	*10* %	*Steady, non-uniform and gust wind*
Lawson and Penwarden, 1976; Lawson, 1980	*23.7*	*17.2*	*2* %	*Beaufort Scale > Range 7 (14.1–17.2 m/s)*
Melbourne, 1978	*23*	-	*2.5* %	*Gust wind*
Penwarden, Grigg and Rayment, 1978	-	*15–20*	*2* %	*Unpleasant,* U=*8–10 m/s Discomfort,* U=*5 m/s*
Murakami and Deguchi, 1981	*15*	-	-	-
Bottema, Leene and Wisse, 1992	*15-20*	*10*	*2* %	*Young (15 m/s) and elderly (20 m/s) people*
Soligo et al., 1998	*22–27.8*	*11.9–15*	*0.1* %	*Modified Beaufort Scale (1.5 m above the ground)*
Peters, 1999	*12.5–20*	-	-	*depending on gust duration and activity of pedestrians*
NEN, 2006	-	*15*	-	*Based on Lawson's Comfort Criteria and Beaufort modified Scale*
City of London Corporation, 2019; Leeds City Council, 2019	-	*15*	-	

Wind gust values U_g can be measured or computed directly through experimental and/or numerical simulation (Blocken et al., 2016). However, it is far more common to evaluate gust speed indirectly from the mean wind speed U and the measured standard deviation of wind speed σ_u using an expression of the form

$$U_g = U + g\,\sigma_u \qquad (3),$$

where g a multiplying factor called 'peak factor' (City of London Corporation, 2019; Leeds City Council, 2019; NEN, 2006). Table 2 shows that a range of *0-3.5* is reported in literature for g, with no universal agreement exists as to the most suitable value to be used in pedestrian distress criteria (Bottema et al., 1992). In standard practice, especially when using numerical low-fidelity techniques (see Table 1), an *a priori* choice of g is the only way to implement Equation (3). An in-depth argument on the suitability of this approach can be found in recent literature (Blocken et al., 2016).

Table 2. Peak factors suggested for distress criteria as found in literature.

Literature	*g*
Isyumov (1978)	*1.5*
Uematsu et al (1992)	*1.0 - 3.0*
Soligo et al (1998)	*3.5*
Bottema (1993)	*1.0*
Hunt (1976)	*3.0*
Melbourne (1978)	*3.5*
Lawson and Penwarden (1975)	*2.68*

This brief introduction shows that a deeper insight into gust values at pedestrian level wind is needed to gain accurate data to be input in pedestrian level wind safety criteria (Blocken et al., 2016).

The study reported in this paper examines the efficacy of standard techniques used to assess pedestrian level winds. The main focus is on the adequacy of low-fidelity techniques, popular as standard industrial practice, i.e. Irwin probes, and steady Reynolds Averaged Navier Stokes (RANS) and high-fidelity techniques, i.e. hot-wire anemometry and Large Eddy Simulation (LES), in providing cost-efficient but accurate data for the assessment of the effective wind speed U_e. Additionally, the use of topographic bases in wind tunnels (shaped to the contours of the test site) rather than standard flat bases is examined. This study is part of the United Kingdom EPSRC Project 'The safety of pedestrians, cyclists and motor vehicles in highly turbulent urban wind flows', which included full scale measurements, wind tunnel measurements and CFD simulations. In addition a pedestrian and cyclist safety risk framework is also being developed, using measurements on instrumented volunteers walking along a test-route during a strong wind event. Further results from this project will be published in due course.

A background on the various experimental and numerical simulation techniques as applied in literature is given in Section 2, with a focus on low- and high-fidelity techniques. Section 3 describes the methodology of the work, i.e. the full-scale validation test case (3.1), the wind tunnel experiments (3.2) and the numerical models (3.3). Section 4 shows the results in terms of the mean wind speed and the gust wind speed. Section 5 discusses the results in the context of its implications for the future of pedestrian level wind assessments and relevant conclusions for this work are presented in Section 6.

2 Background

Available methods to assess pedestrian level wind (PLW) comprise of both experimental and numerical simulation. A distinction can be made on the fidelity of the different models. Low-fidelity techniques are capable of providing an accurate estimate of the mean wind speed only, with no or partial information on gust values, directionality or fluctuating statistics of the flow. In standard practice and most of literature on PLW low-fidelity techniques are usually implemented. On the other hand, high-fidelity techniques can provide a large amount of information on the fluctuating behaviour of the wind environment. However, they are more expensive and require a significant expertise on the user as guidelines are mostly missing, and hence are not used as industrial

standard. Table 3 lists most available low- and high-fidelity techniques for experimental and numerical simulation, with comments on the advantages and disadvantages of each technique.

*Table 3. Classification of techniques for wind velocity measurement. Techniques used in the present study are marked **

		Low-Fidelity	*High-Fidelity*	*Advantages*	*Disadvantages*
Experimental	*Full Scale*	*Hand-held anemometers* *Cup anemometers*	*Sonic anemometers** *LiDar*	*Real wind and geometry conditions*	*Not available at design stage* *Complex and costly campaign* *Variability of wind conditions* *Coarseness of measurements*
Experimental	*Wind Tunnel*	*Irwin probes** *Multi-hole probes* *Themistors*	*Hot-wire anemometry** *PIV* *LDA*	*Detailing of geometry* *Quick results* *Well established*	*Scaled models only* *Directionality of flow* *Positioning of probes* *Coarseness of measurements*
Numerical	*CFD*	*3D (U)RANS**	*DES* *Hybrid RANS-LES**	*Detailing of geometry* *Quick results* *Well established* *Fineness of measurements*	*Complexity and costs* *Physics modelling* *Validation*

Testing at full-scale to monitor existing PLW conditions is preferable to gain full understanding of the flow. However, such tests are impossible at the design stage, and are normally complex to setup due to practical, health-and-safety, and regulatory issues. As the testing period is normally short, high-wind conditions might not occur during the experimental campaign, resulting in data of limited usefulness (Blocken et al., 2016).

Among the available instruments to measure atmospheric turbulent wind, sonic anemometry (ultrasound pulse based) is a widely used and well-established technique (Cuerva and Sanz-Andrés, 2000; Kaimal, 1979; Nosov et al., 2019). The time Δt, for an acoustic signal to travel the distance s between the transceivers of the anemometer is measured, yielding $\Delta t = s/(c + u)$, where c is the sound speed and u the wind speed. The main limitation of this technique is a dependence on the environmental properties such as air humidity and temperature, which is however eliminated in modern sensors (Hanafusa et al., 1982; Kaimal, 1979). Other limitations include line averaging effects and transducer shadows, which are well known and studied and accounted for (Cuerva and Sanz-Andrés, 2000; Wyngaard et al., 1985).The optimal configuration of the sensors, as developed by Kaimal (1979), greatly overcomes the limitations of sonic anemometry when compared to other types of sensors (Cuerva and Sanz-Andrés, 2000). Sonic Anemometers are able to measure instantaneous 3D velocity components with a high sample rate up to 100 Hz, without the need of moving parts interfering with the flow (as with a cup anemometer, for example) and with negligible effects of the design features (Nosov et al., 2019). They show a linear response, with calibration parameters which stay fixed after setup (Cuerva and Sanz-Andrés, 2000). Sonic anemometry remains the reference for outdoor atmospheric turbulence measurements (Cervenka, 1992).

Experimental or numerical simulations overcome the limitations of full-scale testing by simulating a variety of possible safety-concerning scenarios. Most PLW research uses wind tunnel testing as a reliable standalone assessment tool, with only a few studies offering a validation against full-scale results (Blocken et al., 2016; Jacob and Sagaut, 2018; Mittal et al., 2018). In general, it is shown that wind tunnel simulation is able to generate a fairly reasonable approximation of mean wind speed with a correlation coefficient with full-scale data of about *0.8* (Dye, 1980; Isyumov and Davenport, 1975; Kamei and Maruta, 1979; Visser and Cleijne, 1994; Williams and Wardlaw, 1992). Low-fidelity techniques such as Irwin Probes, and RANS calculations are the industrial standard for the assessment of pedestrian distress and the design of mitigation measures (Blocken et al., 2016). Thermistor type sensors are also widely used in consultancy and some research applications (YinMun et al., 2019). Although high-fidelity techniques such as hot-wire anemometry, LDA, PIV and LES calculations are readily available to the industry for a number of applications (Baker, 2007), the increased accuracy needs to be balanced against increased costs. The higher complexity of numerical high-fidelity setups is also known to increase the risk of macroscopic errors, (Hanjalic, 2005).

2.1 Experimental Simulation

Experimental simulation involves the introduction of a single or of multiple probes in those areas of interest for PLW in a scaled model in wind tunnel testing. As the direction of the wind is generally unimportant when considering PLW comfort, wind speeds (rather than velocities) are typically measured, with Irwin Probes almost exclusively used. The efficacy and application of Irwin probes is well documented in literature (Durgin, 1992; Irwin, 1981; Kuo et al., 2015; Stathopoulos and Wu, 1995; Tsang et al., 2012; Williams and Wardlaw, 1992; Wu and Stathopoulos, 1994, 1993). Irwin probes essentially consist of a larger hole with its end flush with the model ground plane and a smaller middle sensor tube which protrudes above the model surface at height h. The excess pressure at the bottom of the hole over that at the top of the sensor tube, Δp, is measured using differential pressure sensor and from this pressure difference the wind speed at height h can be calculated in accordance to a calibration formula, by assuming that the top of the probe is in the log-law dominated part of the boundary layer (Blocken et al., 2016; Durgin, 1992; Irwin, 1981; Tsang et al., 2012; Tse et al., 2017b, 2017a). Irwin Probes are able to provide a reasonable estimate of mean wind speed and low-frequency speed fluctuations in PLW studies (Irwin, 1981), and have the advantage of being simple and robust to use while their relatively small size allows the installation of numerous sensors onto the model surface with a limited effect on the wind flow. They are also omni-directional, which avoids the need for re-alignment when wind direction changes (Wu and Stathopoulos, 1993). However, it is important to note that Irwin probes might be sensitive to the shape of the boundary layer in the measurement area and their measurements may also be biased in highly intense turbulence >30 % and at wind speeds below ~ 1.5 m/s (Tsang et al., 2012). Furthermore, the frequency response of Irwin probes has similar limitations to that of Pitot tubes, and numerical noise can render measurements unusable at frequencies higher than *10* Hz (Wu and Stathopoulos, 1994). Therefore, Irwin probes have often been employed when mean wind speeds are of primary interests (Durgin, 1992; Tsang et al., 2012; ; Tse et al., 2017a, b). Despite their limitations, Irwin probes remain the standard practice to assess pedestrian level winds both in practice and

research, with recent studies showing the criticality of a correct calibration of the sensors with either Pitot or hot-wire sensors (Zhang et al., 2018; Zheng et al., 2016).

Multi-holes probes, such as the three-hole Cobra Probe or the five- seven- or eighteen-hole Omni-Probe are also commonly used to provide high-resolution measurements of turbulent flows in wind tunnel testing. However, their insensitivity to wind speeds below *2* m/s, and limitations to the directionality of the velocity field limits their scope for PLW. Compared to Irwin Probes, the size of these probes may also be problematic, if compared to the pedestrian level to be measured on scaled models, as a height of *5-10* mm might be of interest in such applications (Jensen, 2004; Wu and Stathopoulos, 1993).

Hot-wire anemometry overcomes limitations of multi-hole probes, as its accuracy does not depend on the measured wind speed, and it is used extensively for a wide range of flows, when high-resolution of measurements and accuracy is needed (Stainback and Nagabushana, 1993). However, hot-wire anemometry is still limited due to the spatial resolution of measurements, the non-simultaneous measurements, and the sensitivity of the probes to the wind direction (Blocken et al., 2016; Durgin, 1992). However, a major advantage of hot-wire anemometry includes the high frequency-response (*>10* kHz, compared to *2* kHz of multi-hole probes and *~500* Hz of Irwin Probes), and the capability for higher spatial resolution due to the small dimensions of hot-wire prongs. Nonetheless, the accuracy of hot-wire anemometry can be affected by the angular changes in the velocity vector normal to the wire axis, hence the positioning of the probe is of extreme importance and not consistent throughout the spatial measurement positions (Durgin, 1992; Castro, 1992). Furthermore, at high turbulence intensities *>30* %, hot-wire anemometry rectifies reverse winds resulting in higher mean wind speed and lower standard deviation measurements (Durgin, 1992; Blocken et al., 2016).

Other high-fidelity methods for wind tunnel testing include Laser Doppler Anemometry (LDA) and Particle Image Velocimetry (PIV), which are rarely used in PLW research due to their cost but also the necessity of measuring close to the ground, which might be a strong limitation for the laser and the seeding particles to reach the measurement area (Conan et al., 2012; Sciacchitano, 2019; Wu and Stathopoulos, 1997).

Information on other possible techniques to test PLW, which are not mentioned in Table 3, can be found in the literature (Blocken et al., 2016).

2.2 Numerical Simulation

Numerical simulation using Computational Fluid Dynamics (CFD) allows the testing of a model geometry in full scale with results available for the whole of the flow field, without introducing disturbances to the measured flow or worrying about similarity (Blocken, 2014). Having the possibility of visualising the full flow field in both space and time is of a great advantage to the interpretation of experimental results, and for this reason the industrial practice is normally to combine wind tunnel testing with preliminary CFD. Three-dimensional Reynolds Averaged Navier-Stokes (RANS) is almost exclusively used in PLW research (Blocken et al., 2016). RANS is the low-fidelity technique for numerical simulation, and it only allows for U and σ_u to be calculated. RANS results in terms of mean wind speed are accurate if the available best practice guidelines are implemented

(Blocken et al., 2016; Franke et al., 2011, 2007). Steady RANS is most commonly implemented for PLW, as unsteady RANS (URANS) is only beneficial when alternating flow patterns such as vortex shedding are examined, which is not the case in urban winds (Blocken et al., 2016). However, the estimation of U_g requires the implementation of Equation (3), and therefore the arbitrary choice of a peak factor *g*. Thus, RANS simulations must always be supported by experiments to estimate a suitable value for *g*. Arguably, it has been noted that this might be a marginal issue, as the variability of *g* is limited in locations where the wind speed is such as to cause distress (Tominaga et al., 2008). However, some authors question this claim and infer that Equation (3) should be avoided to assess pedestrian safety (Jacob and Sagaut, 2018).

High-fidelity numerical techniques include the Large Eddy Simulation (LES) and the hybrid RANS-LES methods, e.g. the Detached Eddy Simulation (DES). LES is known to accurately predict the fluctuating flow behaviour, depending on the resolution of the computational grid, i.e. if a large proportion of the turbulent energy production is resolved (Sagaut, 2006). The grid resolution is a great limitation to the cost-effectiveness of a LES. A state-of-the-art LES would require a mesh having $\Delta \sim \lambda_u$, where $\Delta = \sqrt[3]{dxdydz}$ is the grid size (also cut-off length), and λ_u the microscale of turbulence, which relates to the smallest energy carrying length scales in the flow. Besides the difficult assessment of λ_u without preliminary data, this criterion generally leads to quasi-DNS (Direct Numerical Simulation) with an exponential increase in computational costs (Davidson, 2009). A variety of sub-grid scale (SGS) models has been developed through the years to improve computational cost while retaining accuracy, allowing the use of non-uniform meshes (Blocken, 2015). The Wall-Adaptive Lagrangian-Eulerian (WALE) SGS model is a relatively recent formulation, which overcomes the limitations of the Smagorinsky-Lilly SGS model with regards to anisotropy, without requiring additional computations as for the Germano SGS model (Nicoud and Ducros, 1999). Similarly to Smagorinsky, the WALE SGS model requires the definition of an arbitrary model constant, which is indicated in CFX guidelines as $C_w = 0.35$. C_w has a minor effect on heavily turbulent flows which arise in the built environment, as it regulates the amount of energy dissipated through the antisymmetric part of the velocity tensor close to the wall.

Traditional LES requires turbulent scales of the flow to be solved near the wall, with strict mesh requirements in terms of the dimensionless wall distance y^+, strictly <1. Hybrid RANS-LES approaches have been developed with the aim of easing y^+ requirements. DES is rarely used in PLW research, due to the known complexity of its meshing strategy (Dadioti and Rees, 2017). Wall-Modelled LES (WM-LES) is an alternative hybrid approach where the RANS model is not introduced using a blending function as with DES. Instead, the RANS model is only used at the first cell, and the swap to LES is independent of the nature of the flow field or the mesh resolution (Shur et al., 2008). In principle, a wall distance of $y^+ > 10$ could be used in a similar way as RANS. However, practice shows that it is fundamental to limit mesh coarseness to $y^+ \sim 5$ for reliable results (Blocken, 2018; Hanjalic, 2005; Shur et al., 2008). Grid refinement is among the major challenges preventing a handbook on LES to be readily available, as the potential of the methodology is mostly unknown (Blocken, 2015; Franke et al., 2011). The ratio between LES and RANS in the WM-LES model uniquely depends on y^+, i.e. if $y^+ \sim 1$ WM-LES coincides with standard LES near the wall. This hybrid model still requires a careful building of the

computational grid, but it has the great advantage of avoiding the use of blending functions which are present in DES and known to affect accuracy due to their sensitiveness to grid density variability (Spalart et al., 2006). More details on WM-LES as coded in Ansys CFX/Fluent is available in Shur *et al.* (2008). The computational scheme is also of overwhelming importance in LES. To help convergence without losing accuracy the bounded central differencing scheme (CDS) as coded in CFX is used.

The time step choice is also a delicate aspect for LES. The Courant–Friedrichs–Lewy (CFL) condition for numerical convergence requires the Courant number $Co<1$, where $Co=U\Delta t/\Delta x$, and Δx, Δt and U are here respectively the local cell size, the local through-flow time, and the local flow velocity.

3 Methodology

3.1 Experimental full-scale field test

This work compares the adequacy of experimental and numerical simulation to assess pedestrian safety. Data from a range of wind tunnel and CFD techniques as indicated in Table 3 is validated against full-scale data. These data were collected on the University of Birmingham (UoB) Campus. Figure 2 shows the UoB Campus as of 2015 compared to the computational geometry used for numerical simulation. Relevant landmarks are marked.

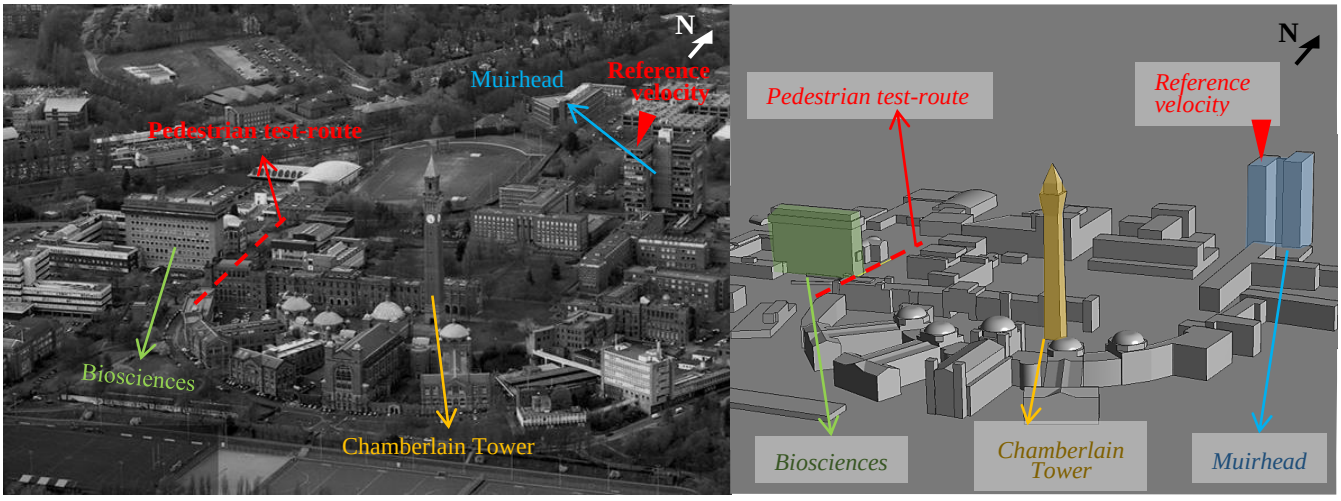

Figure 2. University of Birmingham Campus. (Left) aerial view as of 2015. (Right) view of geometry with landmarks and reference locations.

Storm Ophelia was a major wind event which occurred on 12/10/2017 and which caused significant damage and injury in the United Kingdom and the Republic of Ireland (The Guardian, 2017). In this study, we use data measured between approximately 14:10 and 16:30 during Storm Ophelia, which had a wind direction of South-South-West (SSW, *203°* from North). A reference anemometer (Gill WindMaster) is permanently installed on a *10* m mast on the south-west corner of the roof of the *62* m tall Muirhead Tower (MT), as marked in Figure 2 and Figure 3. Figure 3 shows the eight sonic anemometers used at pedestrian level, and their positions at particularly gusty area near the base of the Biosciences building. The anemometers were at a spacing of *9* m, *5* m from the closest side of the building. All of these anemometers (a mixture of Gill WindMasters and Gill R3-50s) were configured to measure wind speeds at a height of *2* m above the ground. Both reference and pedestrian

level anemometers were set to record three-dimensional velocity data at a sampling rate of *10* Hz. The Gill WindMaster anemometers are capable of measuring wind speed within the range of *0-50* m/s with an accuracy better than *1.5* % of the root mean square (RMS) (Gill Instruments Ltd., 2019). The Gill R3-50s are likewise able to measure wind speed up to *45* m/s, with the same accuracy. Note that although both of these sonic anemometers measure three velocity vectors, only the horizontal wind speeds, given by the vector sum of the two horizontal wind components, are considered in the following analysis since the safety of pedestrians depends predominantly on the horizontal wind component (Blocken and Carmeliet, 2004).

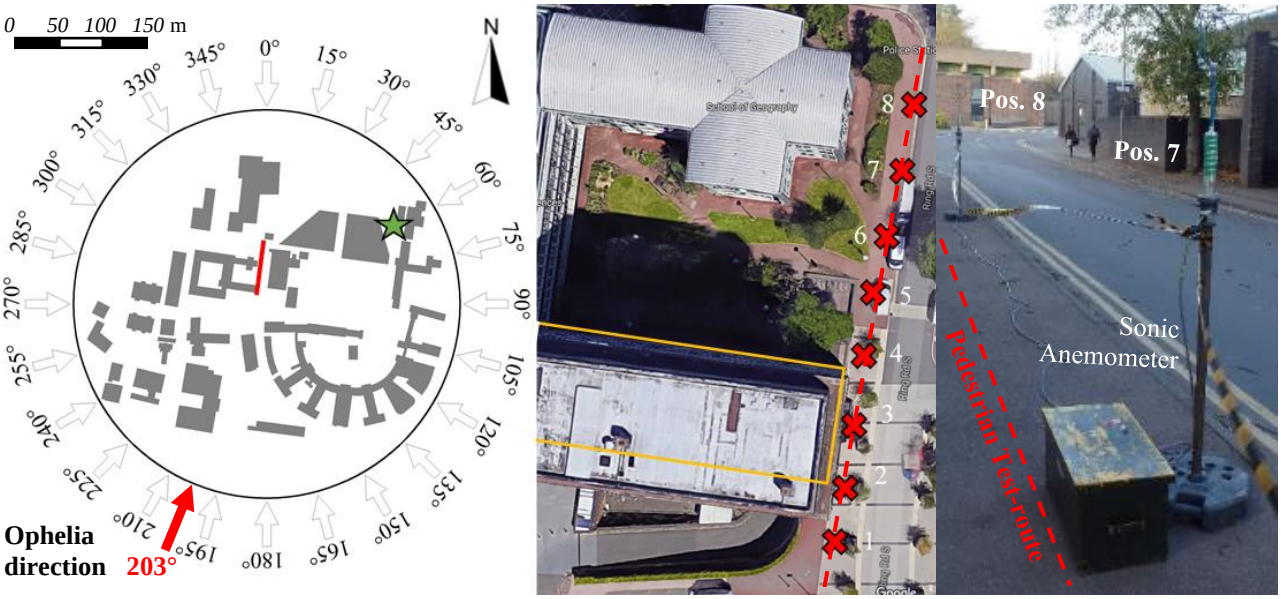

Figure 3. Full Scale Experiment. (Left) Map of UoB campus, with footpath alignment at the base of the BB and reference point position on top of the MT, with cardinal directions; (centre) Aerial view of footpath and position of 8 sonic anemometers (Map data ©2019 Google)*; (Right) view of sonic anemometers as installed during the measurement campaign.*

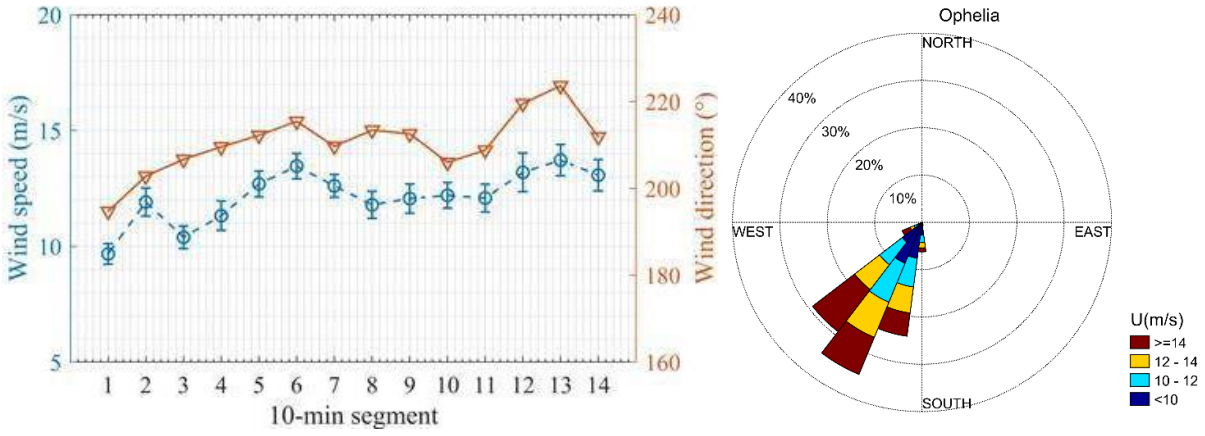

Figure 4. (left) Mean wind speed and wind direction for each 10-min window measured on the 12/10/2017 from 13:10 to 16:30. Error bars show the standard deviation of the wind speed; (right) Wind rose plot at Muirhead Tower based on all 10-min windows, with occurrence of wind speeds.

Figure 4 shows the *14 10*-minute segments mean wind speed and direction, as measured at the reference position above the Muirhead Tower. Each segment contains *6000* individual measurement data. Unless otherwise specified, wind speed parameters given in this paper are the ensemble average of values presented in Figure 4.

This is standard practice for the calculation of bulk statistics of atmospheric turbulent flows (Conan, 2012). Figure 4 shows also the wind rose taken over the entire two-hour dataset, with an average direction of 203°.

3.2 Experimental wind tunnel tests

In wind tunnel tests, both reference and pedestrian level wind speeds have been measured at locations equivalent to those in the full-scale test using various measurement instruments. A Cobra probe has been used to measure the incoming wind speed on top of the model Muirhead Tower, while Irwin probes and hot-wire anemometry have been used independently for the measurements of pedestrian level winds.

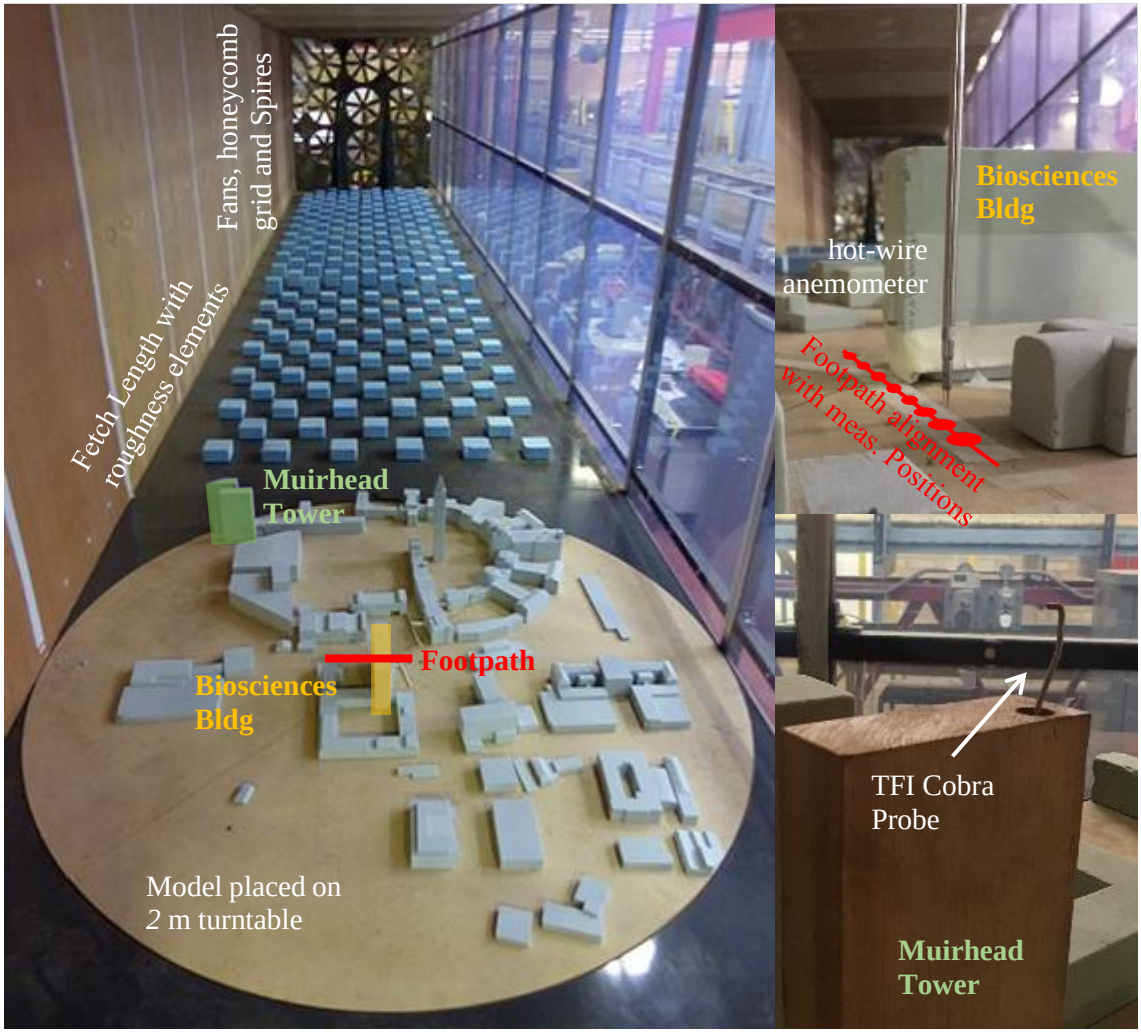

Figure 5. (Left) overview of wind tunnel test setup. (top) HWA placed according to Irwin Probes 8 locations. (Bottom) Cobra Probe for reference point measurement.

The experimental tests were carried out in the University of Birmingham Boundary Layer Wind Tunnel. This wind tunnel is of open-circuit type, with a *2×2* m square working cross-section with a *14* m-long fetch section. The maximum freestream wind speed is *~12* m/s. For wind tunnel simulation of atmospheric flow interaction within an urban area, it is necessary to model both the atmospheric flow and the immediate proximity of the area of concern (Isyumov and Davenport, 1976).

The approaching flow conditions were produced using two triangular spires and an array of surface roughness blocks with two different heights (Figure 5).

The length scale and roughness of the simulation were determined through a range of methods (the integral length scale method of Cook (1978) , calculation of the shear velocity from Reynolds stress measurements combined with curve fitting, pure curve fitting of the velocity distribution). A length scale of approximately *1:300* was determined, with full-scale z_0 values in the range $0.6 \text{ m} \leq z_0 \leq 1.2 \text{ m}$ and a displacement thickness, d, of approximately *3* m. Taking Holmes' (2015) estimate of d as "*about three-quarters of the general rooftop height*", this value seems reasonable given the sub-urban terrain (low-rise buildings) and open areas surrounding the campus. Calculation of the integral length scale from the Muirhead Tower gives a wide range of values over the *10*-minute segments, from *60* m to *600* m with a mean of approximately *200* m. A value of *150* m (full-scale equivalent) was found in the wind tunnel simulations. The power spectrum from the Muirhead anemometer (Figure 6) follows the theoretical "*-5/3*" law, and fits well with the Von Karman spectrum. The turbulence intensity I_u profile is also consistent with the choice of z_0, with $I_u \sim 30$ % at ground level (Figure 7). The wind speed power spectrum, measured at reference height upstream to the model, fits well with the von Kármán model as $R=0.91$ (Figure 7). A circular *1:300* scale model of the relevant area of the UoB campus was used, equivalent to a radius of *600* m at full-scale and having a blockage ratio of *~2* %, calculated by estimating the frontal area of the model at the particular angle of storm Ophelia and comparing it to the cross-section of the wind tunnel. The pedestrian level anemometer positions were approximately at the centre of the campus model, around the south-east corner of the Biosciences building, which was positioned at the centre of the turntable (Figure 5).

Two bases were used, one a standard flat base and the second (the "topographic base") contoured to match the main features of the topography of the test site. Building models and probe positions were identical in the two cases, though only hot-wire probes were used for the topographic base measurements, not Irwin probes.

The Cobra Probe used to measure the reference wind speed (Turbulent Flow Instrumentation Inc., 2015) was fitted on the Muirhead Tower in the same position and equivalent height as the sonic-anemometer at full-scale (Figure 5), thereby providing an equivalent reference velocity for mapping of the wind tunnel results onto the full-scale data. The probe measures 3D velocity data, and was configured to record at a sampling rate of *250* Hz, chosen as a compromise between resolution of time histories and computational cost. The orientation of the Cobra probe head was adjusted to face the approaching flow, i.e. directly upstream into the wind tunnel.

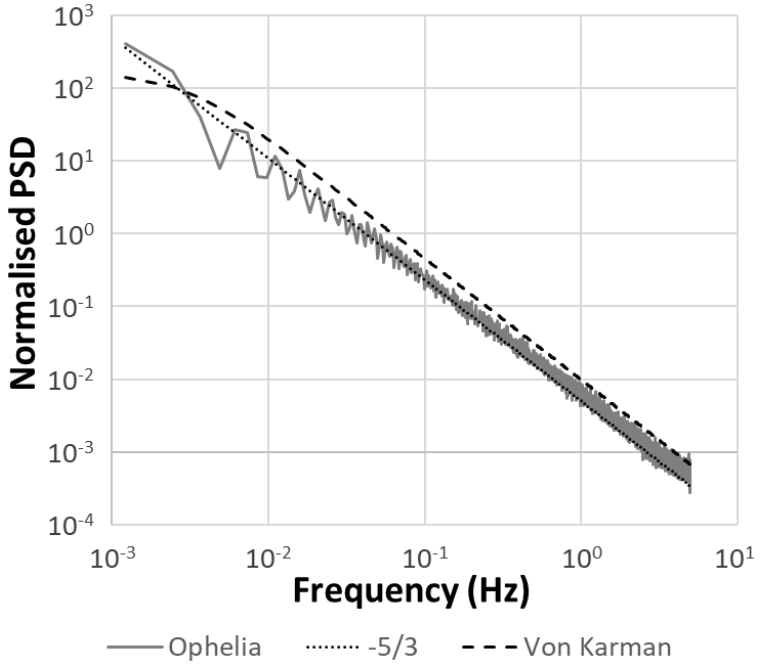

Figure 6. PSD for full-scale data from the Muirhead reference anemometer

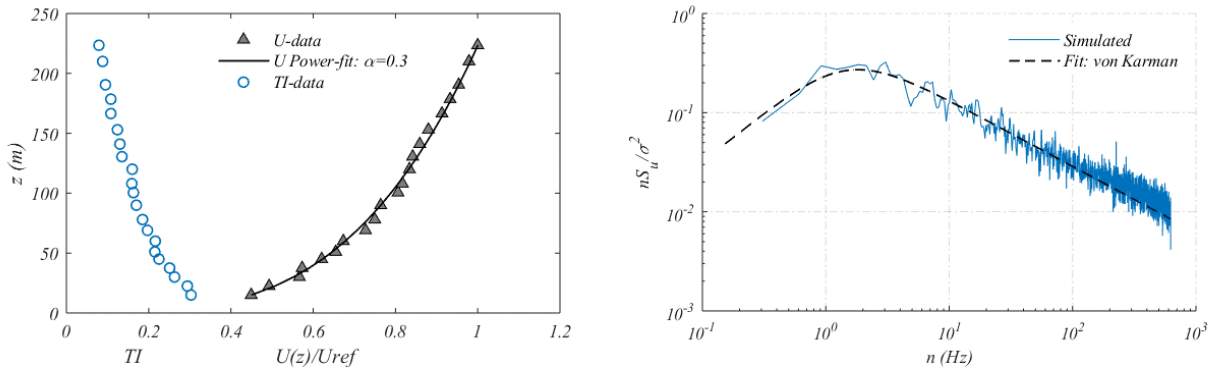

Figure 7. Properties of approaching atmospheric boundary layer (ABL) flow. (Left) vertical profiles of mean wind speed and turbulence intensity; (Right) power spectral density of wind speed measured at reference height upstream the model.

Irwin probes were fitted onto the model surface at locations corresponding to those of the pedestrian level anemometers in the full-scale tests, and connected to a digital pressure measurement system via *0.1 m* long tubes. The pressure difference at each location was measured simultaneously using the LDES025B series digital low differential pressure sensors having a range of ±*25* Pa (First Sensor Ltd., 2019). The pressure sensors were calibrated prior to the tests using a Betz micro-manometer. The Irwin probes used in this study protrude above the model surface by a height of 4 mm, equivalent to *1.2* m in full scale, and the values of model constants α and β (Irwin, 1981) were taken as *0.33* and *1.61* respectively, as specified by RWDI Ltd., the provider of the probes. The differential pressures from the Irwin probes were measured at *50* Hz which, as will be shown below, was sufficient based on the frequency response of the probes. It should be noted that the Irwin probe measurements were performed at a lower height than those in full-scale test (i.e. *2* m) due to their size. However, additional tests were undertaken where wind speed measurements were made in the wind tunnel with a hot-wire

anemometry at full-scale heights of *1.2* m and *2* m, and the differences in the results (not shown) were negligible. Therefore, in the subsequent analysis, no height correction was applied to the wind speed measurements by Irwin probe.

In addition to the Irwin probe measurements, wind speed measurements at pedestrian level were also carried out using a hot-wire anemometry at the same locations. The hot-wire anemometry deployed in the current study was the Tri-axial probe (by Dantec Dynamics Ltd.), which has three mutually perpendicular sensors. The sensors form an orthogonal system with an acceptance cone of *70.4°* (Gökhan Ergin and Velte, 2017). The centre of the hot-wire was positioned at a height equivalent to *2* m in full-scale above the model surface. The sampling rate of the HWA was set to *1000* Hz, found as a good compromise between accuracy and computational cost. Wind speeds were recorded for a time corresponding to *>1* hour in full-scale, or *60* s (ASCE, 2012). This is done in order to estimate statistically stable values of the target wind speed variables. The time scale for wind tunnel and numerical tests is estimated using the geometric scale of the model (1:300) and the velocity scale, which is calculated using the reference wind speed U_{ref} as measured above the Muirhead tower $\left(U_{ref}\right)^{full\text{-}scale} / \left(U_{ref}\right)^{wind\text{-}tunnel} \sim 3$. The time scale is obtained diving the velocity scale by the geometric scale *300/3~100*. This means *1* h in wind tunnel or numerical scale corresponds to *~36* s.

3.3 Numerical tests

A number of numerical simulations were carried out using the commercial code Ansys CFX. RANS and WM-LES techniques are both implemented and their performance compared with both Irwin probes and hot-wire data from the experimental simulation and full-scale data. Both numerical methods are detailed in the following.

The numerical simulation setup replicates the experimental setup, in terms of geometric scale, generation of inlet wind profile, and blockage of wind tunnel walls. A radius of *600* m of the UoB Campus is therefore modelled at a scale of *1:300*, as for the wind tunnel test. The only difference between the experimental and numerical domain is the level of detail of the geometry, which is slightly higher for the numerical case, as noticeable from Figure 2. This is done in order to improve the matching of full-scale conditions, and aligns to guidelines for standard industrial applications (Blocken, 2015).

Figure 8 shows the three computational domains used in this study. In Figure 8 a), the domain replicates a portion of the wind tunnel test section, where only the first *12* rows of the roughness elements are modelled. The domain is prolonged towards the outlet to avoid numerical issues caused by the vicinity of the geometry to the outlet surface. Figure 8 b) and c) show two additional domains, which reproduce respectively the whole wind tunnel fetch length (b) and a conservative domain reproducing the test section only (c). This is done to understand the possibility of matching the inlet wind profile turbulence characteristics as generated in the wind tunnel by means of the geometry or conservatively by deriving boundary conditions from the experimental results. The domains are referred to as truncated, whole and derived in what follows.

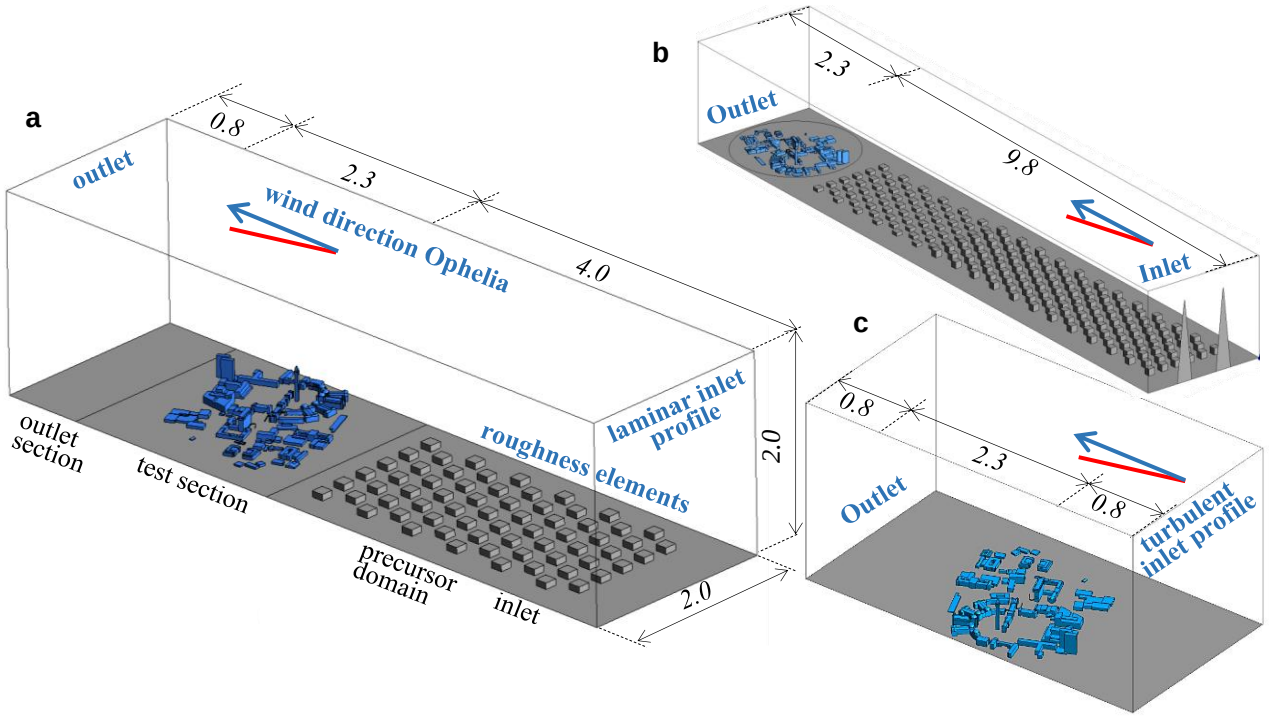

Figure 8. a) Truncated wind tunnel domain with 12 rows of roughness elements. Alternative computational domains: b) whole domain and c) derived derived (*units are in* m). The red line represents the alignment of the pedestrian test-route.

The computational grid is generated for all domains using Ansys ICEM-CFD. It consists of a hybrid unstructured tetrahedral grid. Figure 9 shows the surface mesh topology and the volume mesh in transparency, thanks to a plane sectioning the flow domain. To improve computational costs, the size of the volume cells is intentionally increased greatly compared to the surface mesh (Figure 9).

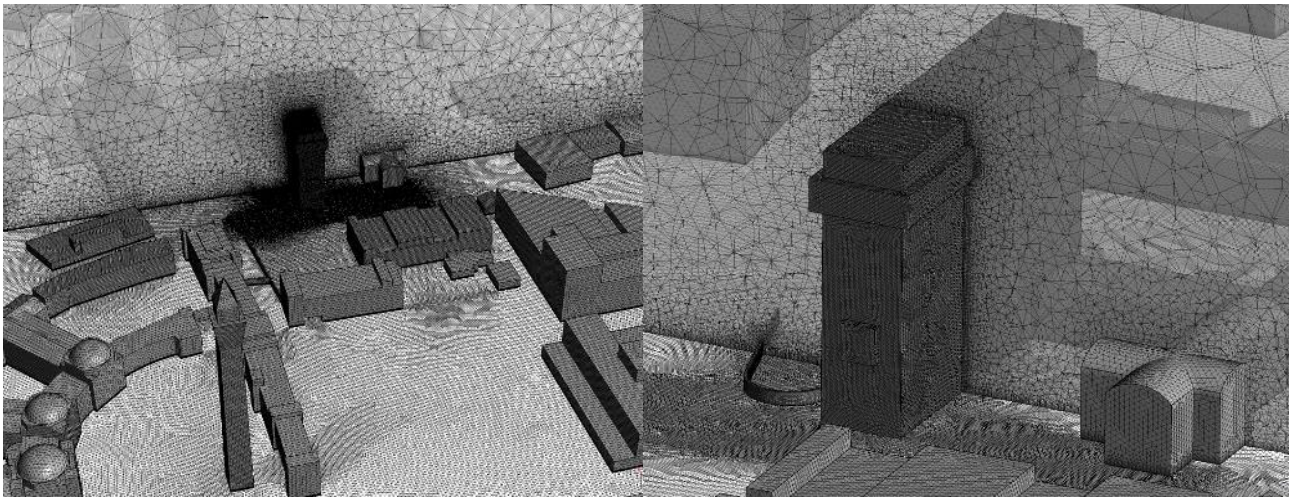

Figure 9. (Left) General view of the computational unstructured mesh, with refined topology along the footpath. (Right) Detail of mesh on the Biosciences Tower.

Considering the full-scale equivalent values, cell-size varies from *~2-5* cm close to the ground, to *~0.1-0.5* m in proximity of the roof of buildings. Further higher from buildings over the UoB campus and the wind tunnel fetch length, the cell size increases up to *~5-10* m. The far-field region of the mesh is coarsened ensuring that the overall size of the computational grid is reduced and a cost effective simulation pursued. Grid topology has

been optimised thanks to a set of preliminary RANS simulations, testing changes in the performance of adaptive wall-functions implemented by RANS and WM-LES due to the quality of the surface mesh. The ground and the Biosciences building feature a boundary layer mesh at their surface, composed of at least *7* prismatic layers. This is to ensure that the first cell lies within the Prandtl boundary sub-layer ($y^+<10$) and velocity gradients are resolved accurately (Blocken, 2015).

Table 4. Computational Setup and grid resolution details

Case	Grid (domain)	Cell size bioscience (m)	Cell size freestream (m)	Cell size pedestrian (m)	Grid size ($\times 10^6$)	Numerical Method	SGS-Turbulence model	Time step Iterations*	CFL number (mean; max)
LESc	Coarse (truncated)	*0.05*	*0.5*	*0.03*	*6.69*	WM-LES	WALE	*0.0005*	3×10^{-4}; *16*
LES	Medium (truncated)	*0.03*	*0.2*	*0.01*	*16.9*	WM-LES	WALE	*0.0005*	8×10^{-5}; *12*
RANS						RANS	*k-ω SST*	**~2000*	-
RANSd	Medium (derived)	*0.03*	*0.2*	*0.01*	*15.1*	RANS	*k-ε RNG* *k-ω SST* *SA*	**~2000*	-
RANSw	Medium (whole)	*0.03*	*0.2*	*0.01*	*21.1*	RANS	*k-ω SST*	**~2000*	-
LESf	Fine (truncated)	*0.02*	*0.1*	*0.01*	*27.9*	WM-LES	WALE	*0.0005*	3×10^{-5}; *6*

Table 4 lists simulations conducted in this study, with details on the computational grid and the numerical setup. RANS results are referred to as RANS, for the truncated wind tunnel test-section, RANSw, for the whole wind tunnel, and RANSd for the derived boundary conditions. LES is only conducted with the truncated domain, and LES results are named after the coarseness of the computational grid, i.e. LESc, for the coarse grid, LES, for the medium one, and LESf, for the finer grid.

The optimal coarseness of the computational grid has been chosen with a mesh independency study, shown in Figure 10. Three different grids have been created for the LES case, with growing refinement. Figure 10 shows the mean U and standard deviation wind speed σ_u at the eight measurement positions used for the pedestrian level wind measurement. The coarsest mesh deviates significantly from the medium and fine meshes, which are themselves very similar. For this reason, only results from the medium grid resolution LES are considered in the rest of the paper. Table 4 shows further details about the three independency grids together with the grid used for the RANSw case, which follows the medium LES grid specifications.

The models were solved using *7* Haswell computational nodes, each having a RAM of *128* GB and a clock-time of *4.6* GHz over *20* processors. With these resources, simulations took from a minimum of *~2-5* hours for the RANS cases to a maximum of *~10-20* days for the LES cases.

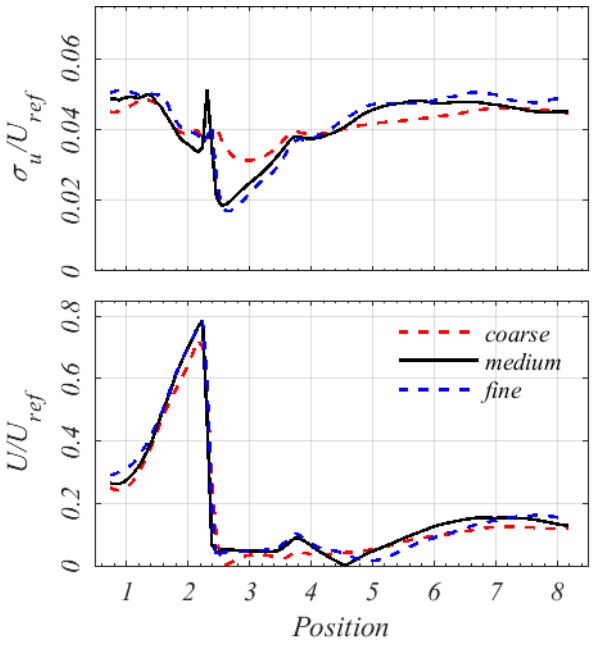

Figure 10. Mesh independency study for LES results: bottom) Mean velocity; top) standard deviation. "Position" corresponds to the anemometer positions shown in Figure 3.

RANS simulations have been carried out for the three domains shown in Figure 8, using a medium mesh resolution as reported in Table 4. The turbulence model of choice is the *k-ω SST* (Shear Stress Transport), which has shown to be performant in predicting the position of the separation and the extension of wakes in bluff body aerodynamics (Blocken, 2014), although not a common choice for pedestrian level studies due to its mesh resolution requirements (Blocken, 2018; Blocken et al., 2016; Mittal et al., 2018). Figure 11 shows that the variability of the mean wind speed *U* as predicted at pedestrian level using a variety of RANS turbulence models, namely the k-ε RNG, k-ω SST, and Spalart-Allmaras (SA), is negligible.

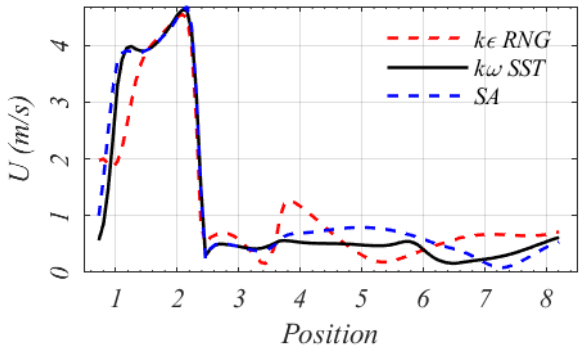

Figure 11. Mean wind speed over pedestrian test-route as computed using the k-ε RNG, k-ω SST, and SA RANS turbulence models for the derived domain RANSd.

The mean wind speed *U* at the inlet boundary condition, as well as the turbulence kinetic energy *K* and eddy dissipation *ε* is directly taken from the experimentally measured wind speed profile in the truncated RANS and derived RANSd domains. For the whole domain RANSw, a constant inlet of *15* m/s is introduced to allow the inlet wind profile to develop through the fetch length. At the outlet, a classic Neumann boundary condition is

used, while all other boundaries have a no-slip condition on the velocity and pressure gradient, as current practice in RANS simulation of the built environment (Blocken, 2015; Franke et al., 2011).

Figure 12 shows the wind speed inflow statistics compared to the experimental wind tunnel measurements. Results are shown upstream of the test section and above the Muirhead tower, where the reference wind speed is measured in full-scale. Figure 12 shows as expected that RANS is not able to solve accurately the turbulence over the roughness fetch length on the wind tunnel, resulting in a deficient mean wind speed profile. However, a gain in terms of the turbulent characteristics is present which might benefit the assessment of pedestrian level winds. On the contrary, a conservative RANS with derived boundary conditions at the inlet shows the closest match in terms of mean wind speed to the experimental measurements. However, the turbulence statistics are underpredicted, especially the turbulence kinetic energy. To provide an inlet wind speed profile with geometry roughness elements creates a closer match in terms of turbulence characteristics at the price of the accuracy of the wind speed profile. Figure 12 also shows the reference wind speed profile as measured above the Muirhead tower. Both RANS and RANSd are close to LES and experimental measurements, while the RANSw case shows an evident shift due to the wind speed profile.

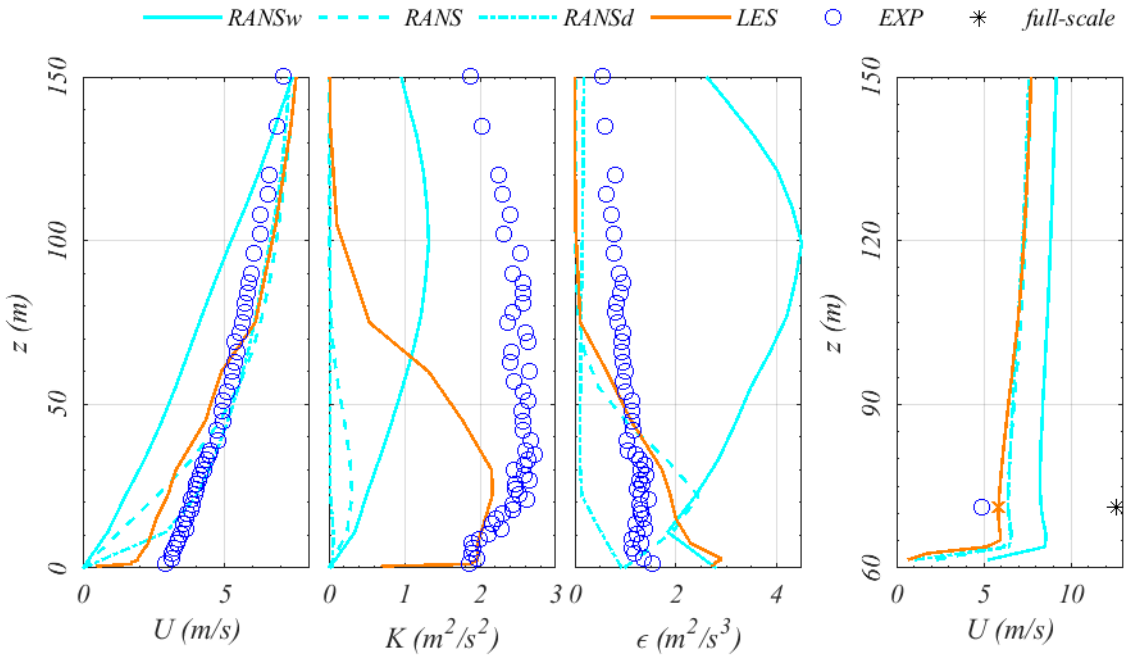

Figure 12 Wind Speed inflow statistics downstream of precursor domain (if present). From left: mean wind speed U, turbulent kinetic energy K and turbulence eddy dissipation ε. (Right) Wind speed profile as measured above the roof of the Muirhead tower, used to calculate the reference wind speed U_{ref}.

The WM-LES setup poses particular attention to the turbulent inlet boundary condition. The mean wind speed profile as measured experimentally is introduced directly at the inlet boundary, in the same way as done in the RANS setup. Inevitably, this leads to the evident mismatch shown in Figure 12 (left), as the effect of the truncated fetch length is noticeable in the mean wind speed profile. However, the match between experimental and numerical values increases with the height, with similar values at the height of the biosciences building. it has been verified *a posteriori* that the mismatch shown in Figure 12 does not affect the accuracy of the numerical

results at pedestrian level. This approach proves effective due to the great benefit of providing a suitable inlet turbulence profile, generated through the roughness elements shown in Figure 8. This turbulence generation approach falls into the category of precursor simulation domain (Tabor and Baba-Ahmadi, 2010). This approach has proved very effective in increasing the accuracy of numerical data against full-scale tests (Chaudhari et al., 2016). The effect of the *12* rows of roughness element is visibly affecting the inlet mean wind speed profile, which for the considered height shows poor agreement with experimental data (Figure 12, left). However, this mismatch does not seem to affect the results shown in Section 4, and this might be due to the fact that PLW flow is mostly influenced by the aerodynamics of the building rather than the undisturbed inlet wind profile measured upstream to the model. It is also worth mentioning that the numerical profile is obtained contextually with the campus model, while the wind tunnel profile is measured in the absence of the model. The issue of the matching of the inlet wind speed is mostly unexplored in PLW, as LES is rarely implemented, and when it is a laminar inlet wind profile is commonly used combined with a fetch length to develop turbulence. However, more studies might be needed to establish guidelines on the introduction of suitable turbulent inlet in LES simulations of PLW.

To ensure the stability of the solution, a time step of $dt=0.0005$ s is set up and the relevant CFL number is shown in Table 4. A simulation time of $T_g=15$ s, which is analogous to ~*25* min in full scale, is found to be a good compromise between statistical stationarity of results and cost-effectiveness of the simulation.

3.4 Estimation of Gust Wind Speed

Gust wind speeds can be estimated using different methods, depending on the available level of detail of the physical or numerical simulation. The following methods have been implemented in this study.

The ***effective gust wind speed*** is derived indirectly from the local wind velocity mean and standard deviation, according to Equation (3). This method is the only option available for RANS data, as only U and σ_u can be calculated. σ_u needs to be evaluated from the computed turbulent kinetic energy, k, using:

$$\sigma_u = \sqrt{(2/3)\,k} \tag{4}$$

where *2/3* comes from the isotropic turbulence assumption. In the highly fluctuating flow at the base of a high-rise building, this assumption might be invalid, further affecting the estimation of the gust speed. The peak factor g is chosen referring to the range of values reported in Table 2. To understand whether a value found in literature is more performant than another, two values for g are considered when implementing Equation (3), namely $g = 2$ and $g = 3.5$. These values are applied consistently to all eight measurement positions.

The most widely adopted method to calculate gust wind speed is based on a ***moving average mean*** from time-varying data with total duration T_g, using a suitable window of length t_g, which is the gust duration. To obtain the representative gust wind speed, time varying data are re-ranked in descending order and the 99^{th} percentile is adopted as the gust wind speed:

$$u_{t_g,T_g} = 99^{th} \left(\sum_{i=1}^{N} u(t_i) \right) \quad (5)$$

where N is the total number of time-steps within a window of length t_g. This method is equivalent to low-pass filtering the data at a frequency of $1/t_g$ Hz and take the percentile of the obtained time history.

This method is preferably applied to stationary time-series (i.e. wind tunnel results or full-scale data with a duration of *10* min). All tests but RANS provide u time-histories. Gust values are found calculating the 99^{th} percentile of measurements rather than the maximum value, using the t-digest routine implemented in Matlab. This arrangement is preferred due to the differences in the time-histories from different methods. Because of the balancing between accuracy and cost-effectiveness, full-scale, experimental and numerical time-histories do not have an analogous sampling time T_g. In wind tunnel testing it is customary to take T_g=*1-2* min. In numerical tests, it is instead normal accepted practice to monitor the convergence of statistics in specific locations of interest, and convergence is measured on the varying-window averaged value and not on residuals (Immer, 2016). This method proved effective and justifies the comparison of experimental and numerical data having a different sample-time T_g.

4 Experimental and Numerical Results

Results from this work are presented and discussed in this section. All data are normalised with respect to the mean wind speed as measured for the various techniques at *10* m from the Muirhead tower rooftop. Full-scale data is presented with reference to the average values found for all *10*-minute segments in the four-hour dataset, with overbars indicating the standard deviation of values from each segment. Experimental and numerical results are compared to full-scale data in terms of mean wind speed (Section 4.2); standard deviation of the velocity field (4.3) and gust wind speed (4.4), which is calculated using three gust durations t_g. A calculation of the peak factor is also presented in Section 4.5, in order to assess the adequacy of using simplified Equation (3) for the prediction of gust wind speed.

4.1 Mean Wind Speed

Figure 13 shows the mean wind speed along the test route. Irwin Probes measurements show good agreement with full-scale results, qualitatively following the same trend along measurement positions. However, measurements do not lie quantitatively within the standard deviation range found for the full-scale measurements, except for Positions 2 and 4. Similarly, hot-wire anemometry measurements are closer to full-scale data at positions 2 to 4 and 7.

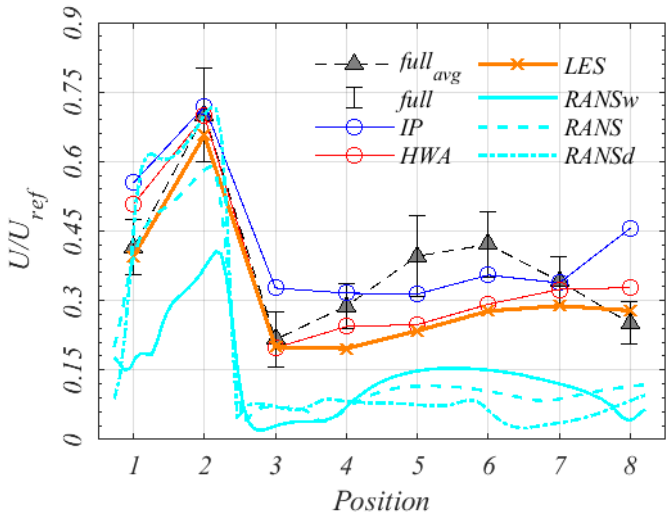

Figure 13. Experimental and numerical Mean Wind Speed against full-scale measurements. Bars indicate the standard deviation of all 10-minute full-scale segments.

Figure 14 suggests a possible reason for this mismatch, as it represents the flow pattern as computed by RANS and LES in terms of flow streamlines projected onto a plane at *z=2* m. The mean wind speed flow field is in agreement qualitatively for both techniques, with RANS underpredicting *U* at all positions (Figure 13). The underprediction of RANS is primarily caused by the vector averaging of RANS which is compared to the scalar averaging of the other methods. Figure 14 shows that position 1 is exposed to a relatively undisturbed flow coming from the inlet wind speed profile through a corridor among buildings. Position 2 on the other hand is in a region of accelerated flow parallel to the western façade of the Biosciences building, while Position 3 is in a region of highly sheared flow, between the region of accelerated flow and a recirculation zone, in which Positions 4 to 7 lie. Position 8 is at the northernmost limits of the recirculation region.

Both Irwin probes and hot-wire anemometry fail to reproduce the full scale results when measurements lie between positions 4 and 7, i.e. within the recirculation region, and at Positions 1 and 8, where the flow is relatively undisturbed from the aerodynamic wake of the Biosciences building.

Figure 14 hints that RANS and LES consistently predict the presence of a large circulation region. However, the core of this region, noticeable close to Position 5 in the LES computation, does not match between the two simulations. This might derive from the unphysical values for *U* predicted by RANS compared to the full-scale data, with an error of *~50* %, as shown in Figure 13. Also LES under-predicts the mean velocity in the circulation region by *~30*%. However only positions *4-6* lie outside of the standard deviation band of the full-scale data. When the whole wind tunnel is modelled in the RANSw case, the performance decreases further. This might depend on the incorrect estimation of the wake downstream of the roughness elements due to the coarseness of the computational grid in that region, which in turn requires additional time-consuming workarounds on the mesh which might not be justifiable in light of RANS results presented in this study. Nevertheless, at position 2 both RANS and RANSd predict the mean wind speed accurately, with a close match to full-scale data. The better prediction of RANSd with respect to RANS may be attributed to the better mean wind speed profile, as shown in Figure 12.

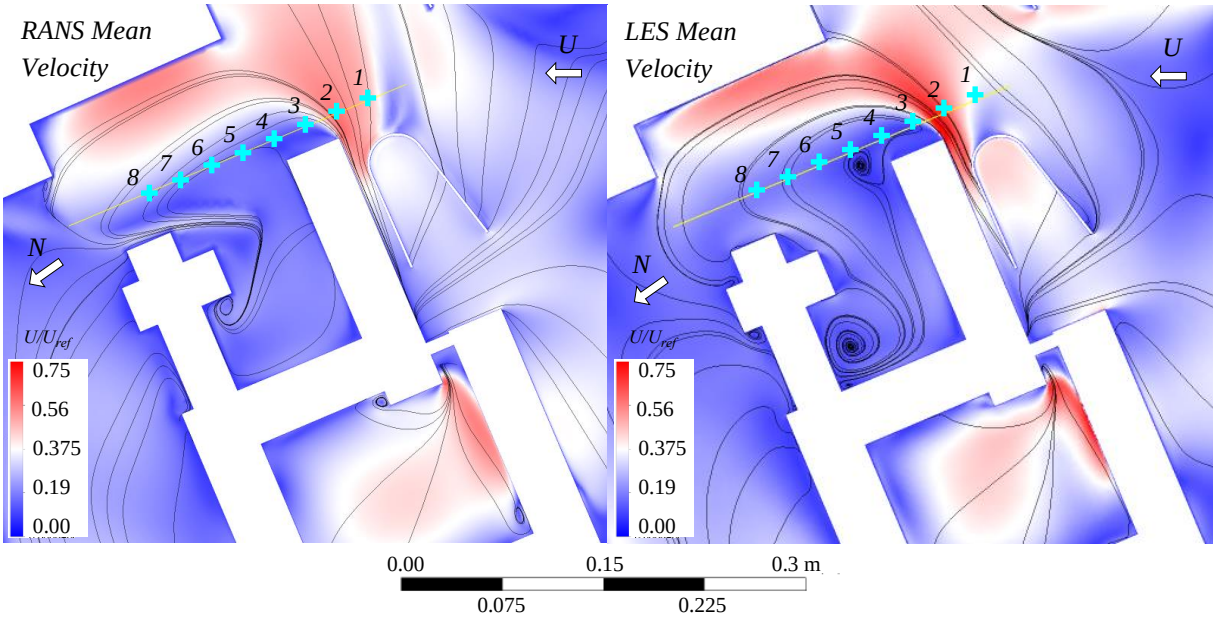

Figure 14. Mean Wind Speed field over the eight measurement positions. (left) RANS case; (right) LES case. Black lines represent mean velocity streamlines.

Consistent with previous findings in literature (Blocken et al., 2016), Figure 14 shows that the agreement with full-scale results is better when the mean wind speed is higher, i.e. in those locations of interest for pedestrian distress. Although this appears to be true in this dataset, there is very little supporting evidence that low mean? wind speeds are a guarantee for potentially safety-concerning gusts not to occur (Jacob and Sagaut, 2018).

4.2 Standard Deviation

Figure 15 shows the standard deviation of the velocity field, which provides an indication of the turbulence behavior along the test route. As stated in the previous section, turbulence can be connected to gust values, and Equation (3), applies. Noticeable deviations occur along the test route for the various techniques. Irwin probes over-predict σ_u at Positions 1 and 2, where the wind speed is highest, while at positions 3 to 7 σ_u lies below the standard deviation of full-scale data. Unlike Irwin probe measurements, hot-wire anemometry tends to under-predict σ_u at all positions, although measurements lie within the full-scale range where the highest wind speeds are observed. However, accuracy decreases radically in the sheared and separated flow regions where hot-wires provide the worst prediction among techniques. This might depend on the directionality of the flow and the limitations of hot-wire anemometry to reverse flows.

RANSw, RANS and RANSd under-predict the standard deviation by over *~80* % at all positions. This might depend on the local anisotropy of the turbulent flow, which cannot be captured by the definition of the turbulent kinetic energy and Equation (4). At position 2, the performance of RANS is slightly superior than RANSd due to the improved turbulent wind speed profile. On the contrary, LES captures the behaviour more closely outside the circulation region, although underestimating σ_u by *~30*% outside of the circulation region. At Position 3 and 4, σ_u is respectively over- and under-predicted, while LES provides the closest match to full-scale data in the circulation region. These positions lie within the highly sheared region of the flow between Position 2 and the

recirculation region, and in general all methods struggle in providing a suitable prediction of the turbulent flow behaviour. For RANS, σ_u is estimated through the turbulent kinetic energy and Equation (4), and Figure 15. shows the evident limits of the technique, with σ_u being underpredicted by *~60* % with respect to full-scale data.

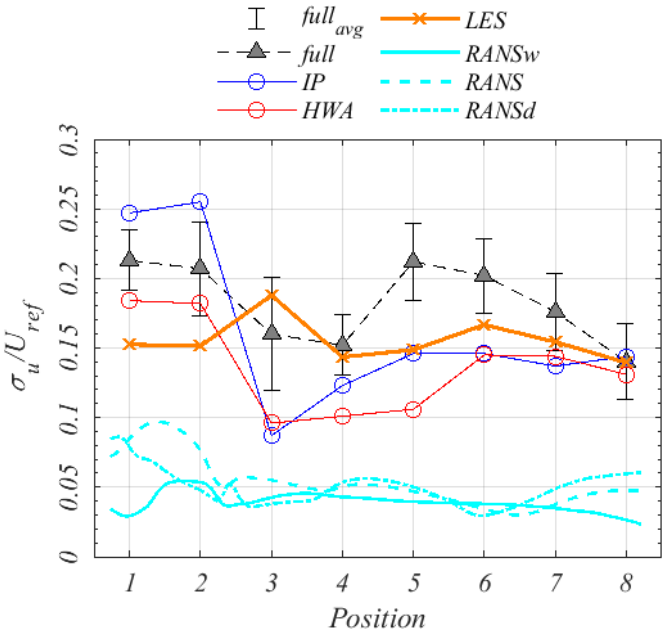

Figure 15. Experimental and numerical standard deviation of Wind Speed against full-scale measurements. Bars indicate the standard deviation of all 10-minute full-scale segments.

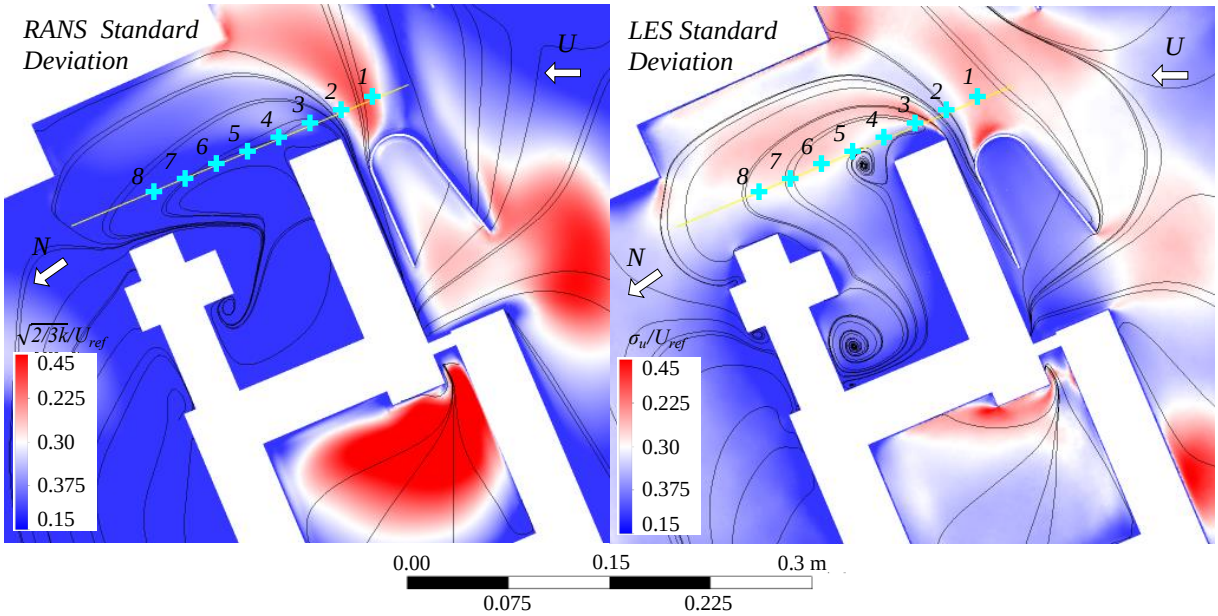

Figure 16. Standard Deviation of Wind Speed field over the eight measurement positions. (left) RANS case; (right) LES case. Black lines represent mean velocity streamlines.

Figure 16 shows the standard deviation flow field. Unlike seen in Figure 14, LES and RANS show rather different results. In the LES case, Position 1 lies in a region of highly fluctuating flow, and this is consistent with RANS. However, Position 2 lies in a region of quieter flow according to LES, which is not at all captured by RANS. RANS also severely under-estimates fluctuations for all the remaining positions. The turbulence environment is important if pedestrian safety criteria based on Equation (3) are to be implemented. As RANS

severely underestimates σ_u at all tested positions, spanning a variety of different turbulent environments, the applicability of RANS to estimate pedestrian level winds might be limited and potentially leading to a misinterpretation of the flow pattern and behaviour.

4.3 Gust Wind Speed

Irwin Probe gust wind speeds are not reported for t_g=*1* s or *3* s. It is suggested in the literature that fluctuations corresponding to *1* s full-scale gusts are not captured by Irwin probes due to the intrinsic limitations of the technique (Wu and Stathopoulos, 1994, 1993). It is also seen in the current research that the power spectra of the Irwin sensors deviate significantly from the hot-wire measurements (and "-*5/3*" line) from a frequency well below that corresponding to *3* s gusts (Figure 17).

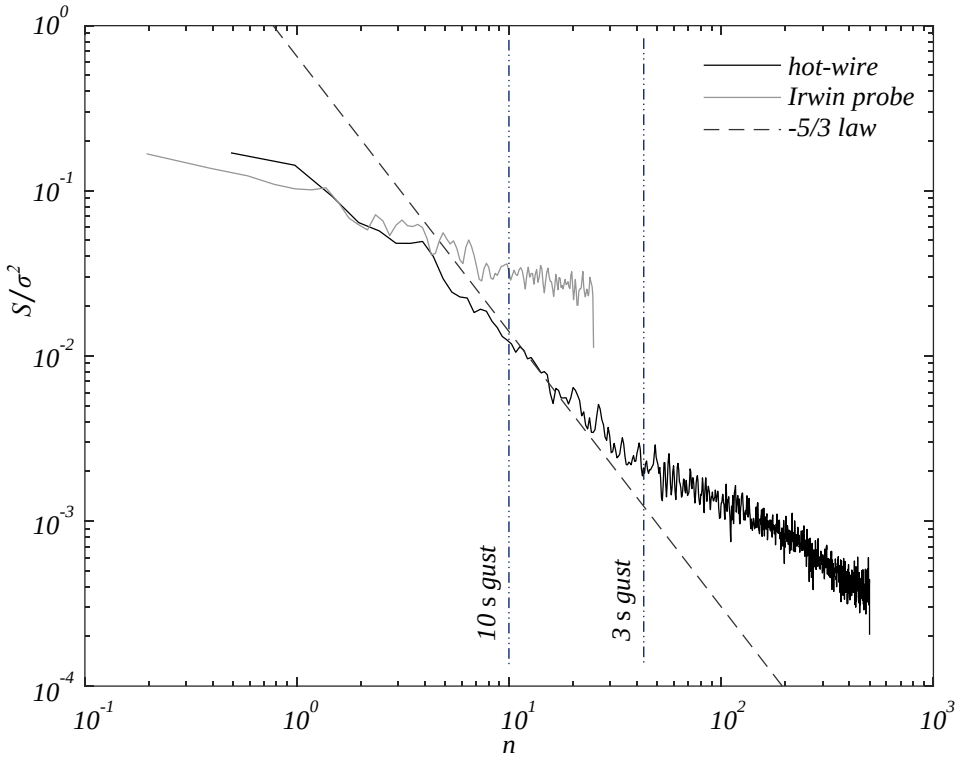

Figure 17 Hot-wire and Irwin probe PSDs at P2. Vertical lines show frequencies equivalent to 10 s *and 3* s *full-scale gusts.*

Figure 18 shows the gust wind speed U_{g,t_g}, calculated using the moving average mean and Equation (5) considering three different gust durations t_g=*1, 3* and *10* s. While *3* s and *10* s gusts are the standard gust speeds reported in wind studies, *1* s gusts have been argued (Jordan et al., 2008) to have an influence on human response, and for this reason are also included in Figure 18 Full scale gust values are computed consistently with experimental and numerical data, and the standard deviation of all *10*-minute segments gust values is plotted in the figure. Alongside directly computed gust values, RANS gust values computed using Equation (3) are also shown in Figure 18, using as peak factor *g=3.5*. Figure 18 shows that Irwin Probes perform rather accurately for a gust duration of *10* s.

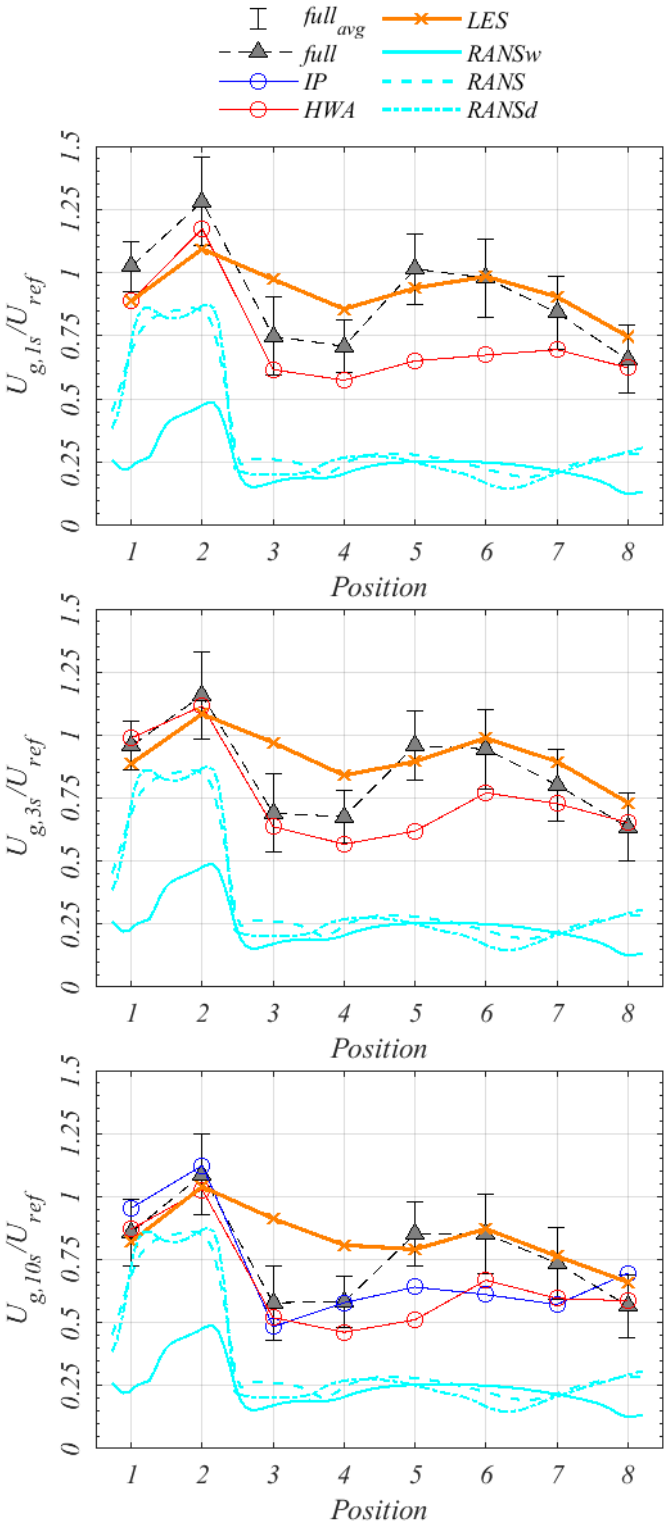

Figure 18. Experimental and numerical Gust Wind Speed against full-scale measurements. Three gust durations are examined: 1 s *(top), 3* s *(centre), and 10* s *(bottom).*

Hot-wire anemometry data supports the argument about the limitation of accuracy of Irwin probes for short gust durations, as good agreement with full-scale data at positions 1-to-4 is found for all t_g values. Differences between experimental results seem to arise from the type of sensor, rather than the flow field. However, within the circulation region, Irwin probes outperform hot-wire anemometry, and this might depend on their

insensitivity to wind direction, which is a problematic aspect for hot-wire probes, as they have to be placed facing the main direction of the flow.

LES predicts the behaviour accurately, with only Positions 3 and 4 lying outside of the standard deviation of full-scale gust values, with an overshoot of ~*30*% noticeable for all gust durations. The low wind speed in the sheared region of the flow might be responsible for this. Arguably, a finer mesh or smaller time-step might solve the issue, but the work is concerned with pedestrian distress, and these points are those which measure the lowest gust speed values in the dataset: a compromise between the accuracy of least-affecting quantities with the cost-effectiveness of the simulation seems only appropriate.

RANS and RANSd only come close to full-scale data at positions 1 and 2, and this is reassuring about the use of RANS to perform conceptual design and evaluations where the flow is easier to detect, as argued in previous literature (Blocken et al., 2016; Tominaga et al., 2008; Yoshie et al., 2007). The similar value predicted by RANS and RANSd might depend on the better prediction of respectively the standard deviation and the mean wind speed, which confirms the importance of predicting turbulence characteristics of the atmospheric inflow.

Excepting Irwin probes, the accuracy of experimental and numerical methods increases with the gust duration. LES is shown to be more versatile in the circulation region, as it is the only technique which allows gust values to be accurately predicted. In the sheared flow region, experimental methods are superior, but time-consuming adjusting of the position of hot-wires is required to increase accuracy.

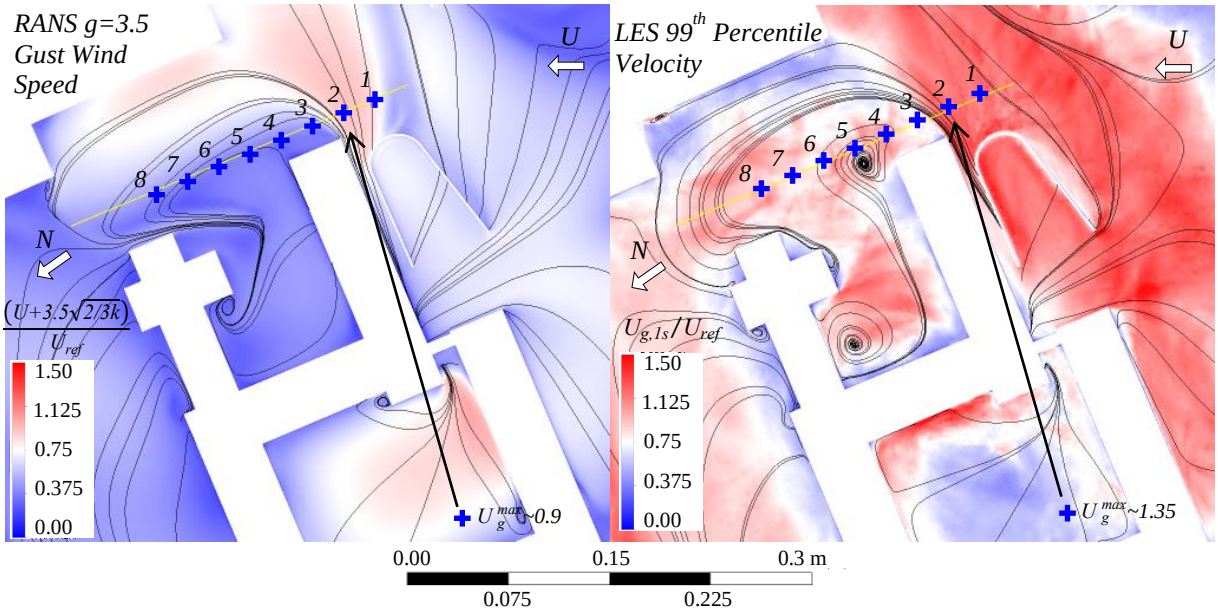

Figure 19. Gust Wind Speed flow pattern over the eight measurement positions. (left) RANS case, computed using Equation (3); and (right) LES case, showing the 1 s 99th percentile gust value. Black lines represent mean velocity streamlines.

Figure 19 shows the flow pattern as computed in both numerical simulations, with the *99th* percentile of the fluctuating wind speed of the LES case on the right. Positions 1 and 2 experience the highest gust values, with U/U_{ref} *~1.45*, equal to *~18* m/s in full-scale compared to a reference velocity of *~12.5* m/s. For the remaining positions, gust values approach the reference mean wind speed U/U_{ref} *~1*, with values up to *~12* m/s being commonly found within the circulation region. This further confirms that highly swirling flows might cause

gustiness and distress to pedestrians, and it needs to be assessed under a risk assessment framework. Figure 19 also shows the correspondence between augmented mean velocity and gustiness, which might justify the use of RANS at early stages of design and the use of Equation (3) to detect critical locations.

4.4 Peak Factor

The gust wind speed is the most important variable to assess pedestrian distress. However, practitioners usually rely on the mean wind speed to work out the gust value: as shown in the previous section, gust wind speed might be tricky to estimate using Irwin Probes, and not possible to obtain using RANS, both popular tools for pedestrian level wind assessment. In that case, the peak factor g is used to work out gust wind speeds from known flow quantities, i.e. the mean wind speed and its standard deviation, or turbulence intensity. Figure 20 shows the peak factor as computed using actual gust wind speed measurements from experimental and numerical techniques. The error bars show the effect of the gust duration, with the higher bound referring to $t_g=1$ s and the lower to $t_g=10$ s. The peak factor found for full-scale data aligns to the envelope of values proposed in literature (Table 2), with $g\sim2.7$ calculated for positions 1 and 2 and in the circulation region, where $g\sim2.8$, consistent with previous findings (Lawson and Penwarden, 1976; Uematsu et al., 1992). At position 3, in the sheared flow region, the peak factor yields $g\sim3.4$, possibly due to intermittency in the flow. The gust duration has a weak effect on the peak factor as values vary by *~10* % and *~15 %* respectively for shorter and longer durations. At positions 1 and 2, Irwin probes yield $g\sim2.75$, which shows they are rather accurate in higher wind speeds, while hot-wire anemometry and LES underestimate $g\sim2.4$. In the circulation region, all methods struggle in matching the full-scale data, with the exception of LES at positions 3 and 7-8. Hot-wire anemometry in particular greatly overestimates the peak factor by *~80* % in the circulation region, which might be caused by the under-prediction of the standard deviation noticeable in Figure 15, which might itself be due to the difficulty in positioning the probe in a highly sheared flow. In the circulation region, all methods show an increased accuracy, with the peak factor decreasing towards full-scale values. As for the range of the envelope of gust durations, Irwin probe data strongly underestimates the peak factor for *10* s gusts, while hot-wire anemometry and LES are consistent with full-scale data, with *1* s values close to *3* s values.

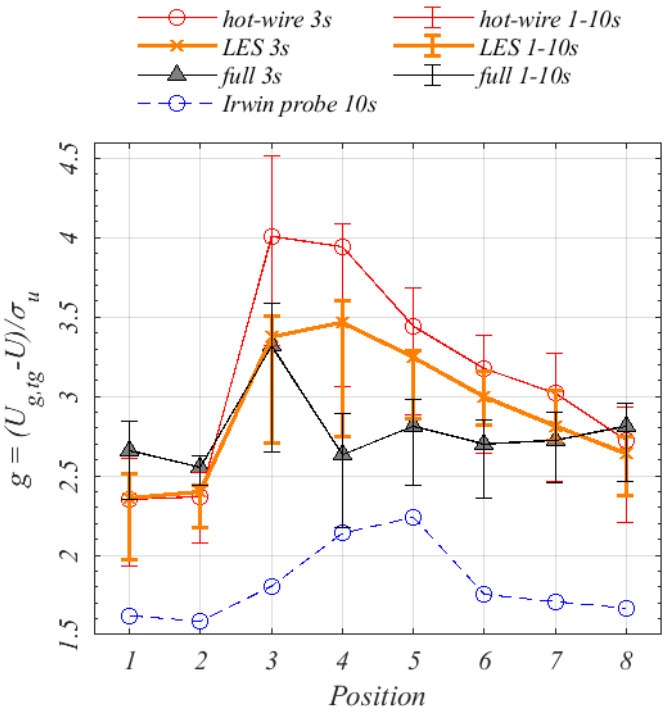

Figure 20. Peak factor g, as predicted with gust wind speeds $U_{g,tg}$ for Irwin probes, hot-wire anemometry, and LES, compared to full-scale. The error bars show the gust duration effect on the peak value, with upper and lower bars showing respectively the 1 s *and 10* s *gusts.*

4.5 Topographic Base

The influence of local topography on wind speed is well recognised in the cases of hills and escarpments (Lubitz and White, 2007; Miller and Davenport, 1998; Wieringa, 1986), but is generally neglected in PLW assessments. The results of the current study, show that the dependence of PLW characteristics on the reproduction of surrounding topographic features is limited, with a difference of *15* % and *11* % seen in the mean *1* s and *3*s gust speeds (Figure 21). This is negligible relative to the full-scale range (Figure 21). The comparison of turbulence intensity and gust factor also lie mostly within *10* % (Figure 22). While the campus has a moderate level of undulation, it should be noted that for particularly hilly cities the benefits of a topographic base may be non-negligible.

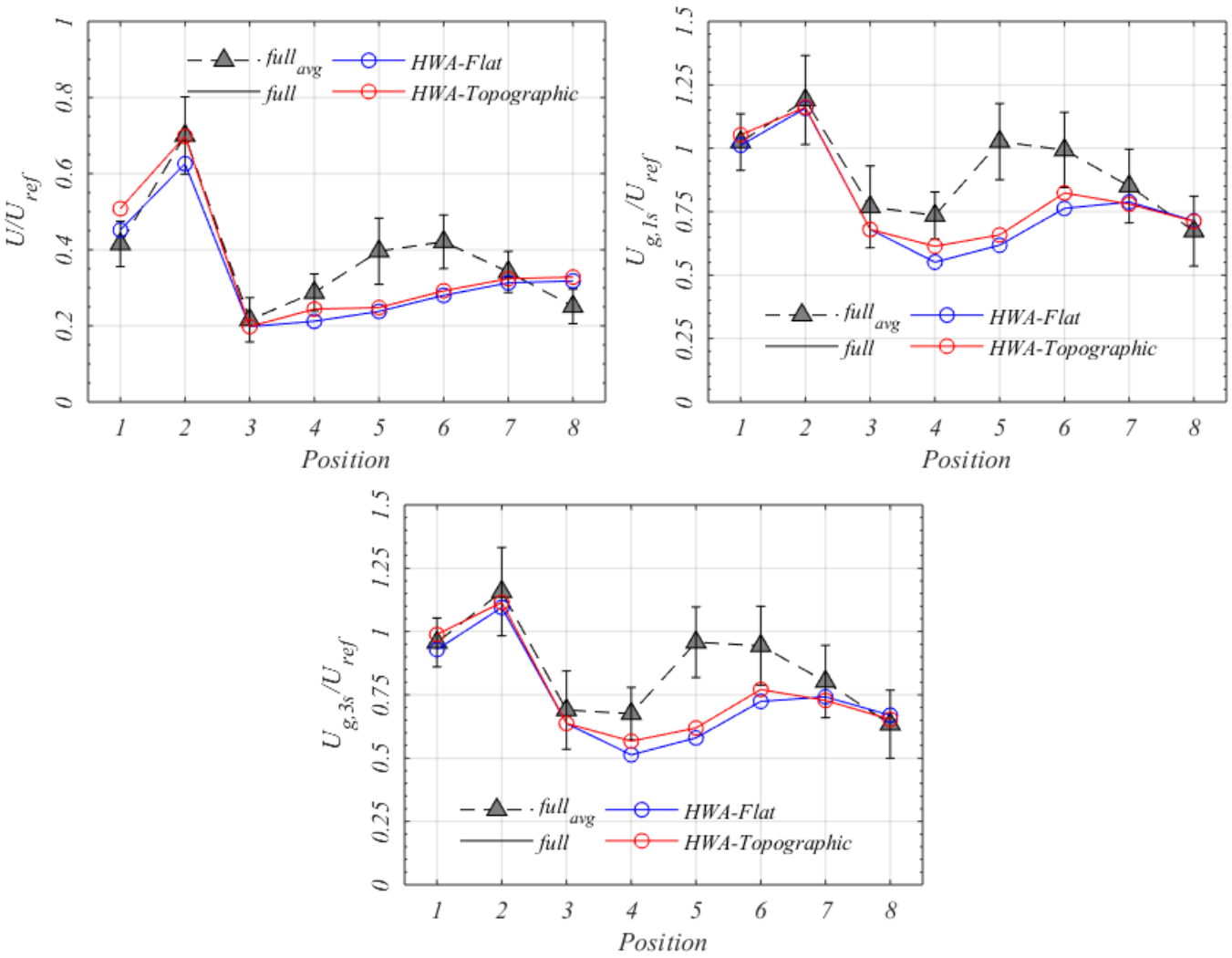

Figure 21. Normalized mean, 1s and 3s gust wind speeds for flat and topographic model tests.

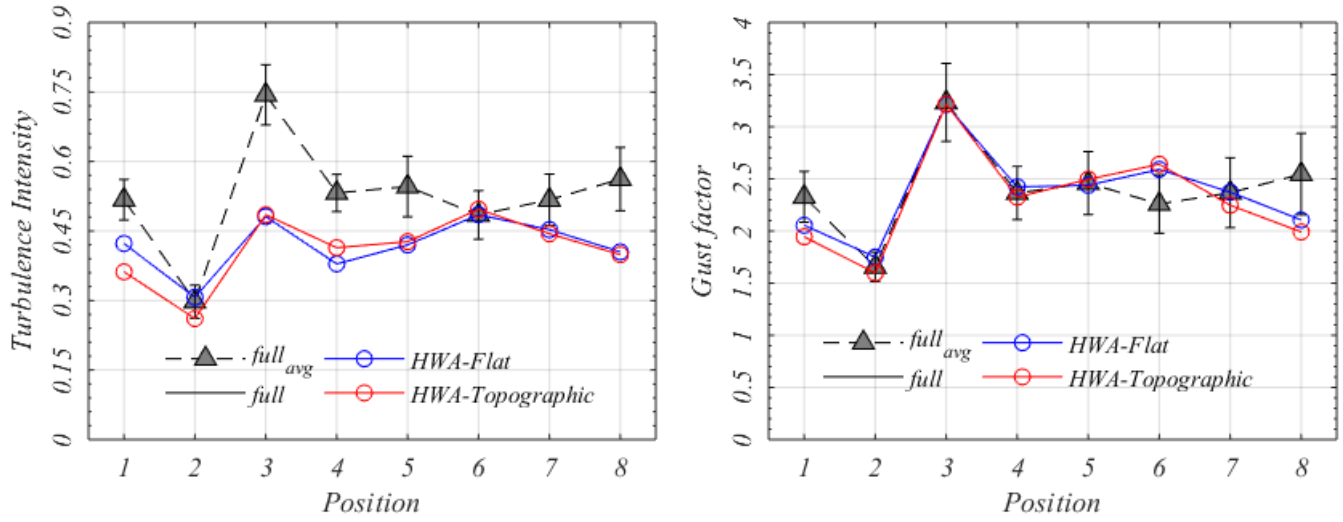

Figure 22. Turbulence intensity and gust factor for flat and topographic model tests.

Table 5. Comparison of topographic model test results (R_T) with flat model test (R_F) results.

	R_T/R_F							
Position	*1*	*2*	*3*	*4*	*5*	*6*	*7*	*8*
Mean Speed	*1.12*	*1.12*	*1.00*	*1.15*	*1.04*	*1.04*	*1.04*	*1.03*
1s Gust Speed	*1.04*	*1.00*	*1.00*	*1.11*	*1.07*	*1.08*	*0.99*	*1.00*
3s Gust Speed	*1.06*	*1.02*	*1.00*	*1.11*	*1.07*	*1.06*	*0.98*	*0.98*
TI	*0.86*	*0.85*	*1.01*	*1.09*	*1.02*	*1.02*	*0.98*	*0.99*
GF	*0.95*	*0.91*	*1.00*	*0.96*	*1.02*	*1.02*	*0.95*	*0.95*

Based on these findings, only data from the flat base is considered in the remainder of this paper.

5 Discussion

Results show that the adequacy of tested methodologies to predict pedestrian level winds varies with the position considered along the test route. Figure 23 shows a 3D view of the pedestrian test-route used in this study. Velocity streamlines show a quite complex flow environment. Wind from the Storm Ophelia hits the biosciences building at an angle of 203 degrees to North. The flow is redirected towards the base of the building, in a downwash, which causes a jet to occur at the southern corner of the building, corresponding with position 2. A circulation region on the downstream side of the building forms due to the large adverse pressure on the leeward side of the building, which affects all remaining positions. At position 8, the wake flow starts to recover with the free stream undisturbed flow north to the biosciences building complex. This is a well-known mechanism in building aerodynamics, and it takes place regardless the direction of the wind. A region of relatively undisturbed, accelerated, circulating and wake flow is always present at pedestrian level in the vicinity of tall buildings (or elongated ground-mounted bluff bodies) (Cermak, 1976; Jesson et al., 2015; Roshko, 1993).

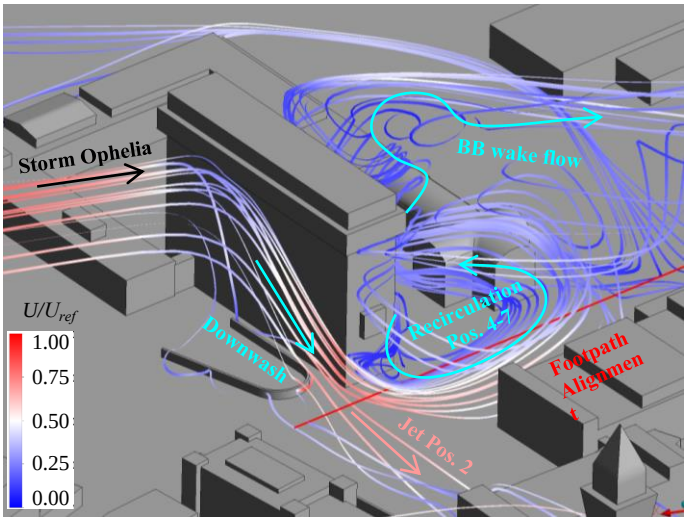

Figure 23. Flow pattern along the footpath, showing the downwash at the Biosciences building southern façade with the jet nearby Position 2, the recirculation region which affects Positions 4-to-7 and the wake flow at the northern side. Streamlines are coloured with the mean wind speed.

All methods perform relatively well at position 2, where mean wind speed is the highest and turbulence intensity lowest of the dataset, and both LES and hot-wire anemometry provide a match within the standard deviation of

full-scale data, with ~*5-10* % error, for all flow quantities. Irwin probes are also capable of predicting flow quantities in these positions, with a larger error of ~*15-20* % (consistent with the variability of full-scale data). At Positions 3 to 4, LES is challenged, as it over-predicts the energy fluctuation, while Irwin probes and hot-wire anemometry provide a reliable description of the gust wind speed. However, in the circulation region LES outperforms experimental methods in terms of gust wind speed, although Irwin probes have a smaller error for the mean wind speed. RANS underperforms in all cases, with only a qualitative account of the physics of the flow, as it correctly estimates the position of accelerated and circulating flow regions, without accurately modelling quantities of interest for the assessment of pedestrian distress.

Table 6 compares the accuracy of calculated numerical and experimental flow variables with respect to full-scale data in terms of correlation coefficient R^2. The relevant bulk statistics for every position is fitted with the respective full-scale value and the correlation coefficient for the least square fit of values is calculated.

*Table 6. Correlation coefficients of experimental and numerical data with full-scale measurements for respectively U, σ_u, and $U_{g,tg}$. *calculated using g=3.5*

	R^2 *Correlation Coefficients with full-scale data*				
	U/U_{ref}	σ_u/U_{ref}	u_{1s}/U_{ref}	u_{3s}/U_{ref}	u_{10s}/U_{ref}
Irwin Probe	0.60	0.42	-	-	0.81
Hot-wire Anemometry	0.74	0.56	0.81	0.82	0.87
LES	0.82	0.47	0.73	0.76	0.86
RANS (RANSw)	0.42	0.32	-	0.37*	-

The advantages and disadvantages of both numerical and experimental methods do not show that one particular technique is preferable to the other. It rather seems obvious from present results that low-fidelity techniques should be instrumental for the design of high-fidelity tests, as suggested in literature (Blocken et al., 2016). However, no mean experimental and numerical low-fidelity techniques can be considered a standalone design tool, and a careful evaluation of the gust wind speed should be implemented when low-fidelity analyses show regions of accelerated flow (Jacob and Sagaut, 2018). The performance of high-fidelity numerical methods is bound to the balance between the cost-effectiveness and accuracy: the setup proposed in this study seems a good compromise, where grid resolution and duration of the time sample seem only to affect performance in the sheared region of the flow, which is not much of interest for pedestrian level winds. Measurements in the circulation region are particularly cumbersome for experimental high-fidelity methods. Full-scale data in this study show that gust wind speed in the circulation region might reach values up to what is measured on top of a high-rise building, i.e. $U_g \sim U_{ref}$ or *12-13* m/s, which might cause distress to a group of vulnerable pedestrians (Bottema, 2000). However, experimental techniques strongly underestimate this value.

The use of the peak factor as a design tool should be strictly related to the knowledge of the flow pattern, as it shows variability along the test route in full-scale. All methods strongly overestimate the peak factor, showing that they all under-predict turbulence. Nevertheless, performance is acceptable in accelerated flow regions and the peak factor is adequate in those (Blocken et al., 2016; Mittal et al., 2018)

A correspondence between the accuracy in the prediction of the turbulent environment σ_u and the gust wind speed suggests that in-depth knowledge of the turbulent environment might be key to improve accuracy.

Another interesting aspect of this work is the role of the atmospheric wind speed profile. The various RANS simulations yield a strong variability and generally a mismatch of inlet conditions when compared to wind tunnel data. This also applies to LES, as shown in Figure 12. Furthermore, there is no guarantee that the wind tunnel profile has any correspondence to the real full-scale profile during the day of the storm Ophelia. This seems to suggest that pedestrian wind conditions are affected by the flow pattern in the immediate vicinity of the building of interest. More research might shed further light on the role of the inflow on pedestrian level winds.

6 Conclusions

The UK EPSRC Project 'The safety of pedestrians, cyclists and motor vehicles in highly turbulent urban wind flows' is aimed at testing low fidelity and high fidelity experimental and numerical techniques in their adequacy in predicting Pedestrian Level Wind to assess distress. In literature, several criteria are based on the assessment of the gust wind speed, which is normally measured directly using high-fidelity techniques or worked out from statistical relations using low-fidelity techniques. It is commonly accepted practice to use less accurate methods to retrieve gust values through indirect calculations, such as the equivalent gust speed, based on the mean velocity and the standard deviation. This research compares a full-scale field test carried out at the University of Birmingham Campus to experimental and numerical techniques, specifically Irwin Probes, hot-wire anemometry, LES and RANS. Low-fidelity methods provide good prediction of the mean velocity. However, this study shows that they are not a guarantee for a reliable prediction of gust wind speed and therefore the risk for pedestrian distress.

For the first time, this study demonstrates the correlation between turbulence at pedestrian level and gust values. In fact, the accuracy of low-fidelity techniques might be unsatisfying also for low order statistics, such as the standard deviation. Wind tunnel tests show that hot-wire anemometry is somewhat more accurate than Irwin Probes, although not seriously out-performing them, suggesting that wind tunnel testing might benefit from Irwin probes further as they do not pose the practical difficulties associated with placing hot-wires in a scaled geometry close to the ground. On the contrary, numerical tests show that the switch to high-fidelity methods is highly beneficial, as the gust speed can be directly computed instead of being hypothesised, based on *a priori* assumptions on the peak factor of a signal. To aid practitioners in using low-fidelity techniques, a simplified approach is proposed for the assumption of a peak factor from environmental turbulent characteristics. This means in turn that the peak factor is to be treated as a space-varying quantity of the flow. In windy areas, where the mean velocity might point out to potential distress, the peak factor is found to tend to $g \sim 2.5\text{-}2.6$. On the contrary in highly turbulent regions of low mean velocity, the peak factor tends to $g \sim 2.7\text{-}2.8$, which suggests that gusts might occur and have a magnitude comparable to windy areas at the limits of circulation regions, as suggested by the presented dataset.

The interpretation of full-scale and experimental results presented in this study greatly benefits from the flow pattern visualisation, which might help to individuate strategies of wind speed containment from the earliest design phases.

This article is the first step of a broad research, which investigates the suitability of high-fidelity methods in assessing Pedestrian Level Wind towards the publication of guidelines to practitioners. In particular, the study proposes to address the following further issues:

- The proposal of a more accurate methodology to assess gust wind speeds for numerical and physical simulations;
- The assessment of best-practice for physical simulation in wind tunnel testing using Irwin probes and hot-wire anemometry;
- The assessment of coarse LES as an early design tool outperforming RANS;
- The response of pedestrians to gusty wind in full-scale tests.

This study only analyses a single wind direction at 8 pedestrian positions and as such is limited in providing general applicability to the quantitative results, especially at design stage. More research is therefore deemed necessary to provide a general methodology for the estimation of pedestrian level winds from simple statistics such as the mean wind speed.

7 Acknowledgments

The authors would like to thank the UK Engineering and Physical Science Research Council, which funded the original research on 'The safety of pedestrians, cyclists and motor vehicles in highly turbulent urban wind flows' on which this work is based under grant number EP/M012581/1. The authors are deeply grateful to Dr Stephanie Gillmeier and Dr Dominic Flynn for their role in respectively the conduction of the full-scale experimental campaign and the setup of preliminary computational simulations.

8 References

ASCE, 2012. Wind tunnel testing for buildings and other structures. ASCE Stand. 1–54.

Baker, C., 2015. Risk analysis of pedestrian and vehicle safety in windy environments. J. Wind Eng. Ind. Aerodyn. 147, 283–290.

Baker, C.J., 2007. Wind engineering—Past, present and future. J. Wind Eng. Ind. Aerodyn. 95, 843–870.

BBC, 2017. Wind death in Leeds prompts tower safety fears [WWW Document]. URL https://www.bbc.co.uk/news/uk-england-leeds-12717762

BBC News, 2014. Bridgewater Place wind reduction plans unveiled.

BBC News, 2016. Leeds' Bridgewater Place owners to foot £900,000 wind bill.

Blocken, B., 2014. 50 years of Computational Wind Engineering: Past, present and future. J. Wind Eng. Ind. Aerodyn. 129, 69–102.

Blocken, B., 2015. Computational Fluid Dynamics for urban physics: Importance, scales, possibilities, limitations and ten tips and tricks towards accurate and reliable simulations. Build. Environ. 91, 219–245.

Blocken, B., 2018. LES over RANS in building simulation for outdoor and indoor applications: A foregone conclusion? Build. Simul. 11, 821–870.

Blocken, B., Carmeliet, J., 2004. Pedestrian Wind Environment around Buildings: Literature Review and Practical Examples. J. Therm. ENV. BLDG. SCI 28.

Blocken, B., Stathopoulos, T., van Beeck, J.P.A.J., 2016. Pedestrian-level wind conditions around buildings: Review of wind-tunnel and CFD techniques and their accuracy for wind comfort assessment. Build. Environ. 100, 50–81.

Bottema, M., 2000. A method for optimisation of wind discomfort criteria. Build. Environ. 35, 1–18.

Bottema, M., Leene, J.A., Wisse, J.A., 1992. Towards forecasting of wind comfort. J. Wind Eng. Ind. Aerodyn. 44, 2365–2376.

British Railways Board, 1970. High Speed Tests at Cheddington, Design project no. 80068.

Cammelli, S., Stanfield, R., 2017. Meeting the Challenges of Planning Policy for Wind Microclimate of High-rise Developments in London. Procedia Eng. 198, 43–51.

Cermak, J.E., 1976. Aerodynamics of Buildings. Annu. Rev. Fluid Mech. 8, 75–106.

Cervenka, S., 1992. Selection of anemometer for measurement of wind turbulence ECN-I-92-029. Petten (Netherlands).

Chaudhari, A., Hellsten, A., Hämäläinen, J., 2016. Full-Scale Experimental Validation of Large-Eddy Simulation of Wind Flows over Complex Terrain: The Bolund Hill. Adv. Meteorol. 2016, 1–14.

City of London Corporation, 2019. Wind Microclimate Guidelines for developments in the City of London.

Conan, B., 2012. Wind resource accessment in complex terrain by wind tunnel modelling. Orléans.

Conan, B., van Beeck, J., Aubrun, S., 2012. Sand erosion technique applied to wind resource assessment. J. Wind Eng. Ind. Aerodyn. 104–106, 322–329.

Cook, N.J., 1978. Determination of the model scale factor in wind-tunnel simulations of the adiabatic atmospheric boundary layer. J. Wind Eng. Ind. Aerodyn. 2, 311–321.

Cuerva, A., Sanz-Andrés, A., 2000. On sonic anemometer measurement theory. J. Wind Eng. Ind. Aerodyn. 88, 25–55.

Dadioti, R., Rees, S., 2017. Performance of Detached Eddy Simulation applied to Analysis of a University Campus Wind Environment. Energy Procedia 134, 366–375.

Davidson, L., 2009. Large Eddy Simulations: How to evaluate resolution. Int. J. Heat Fluid Flow 30, 1016–

1025.

Durgin, F.H., 1992. Pedestrian level wind studies at the Wright brothers facility. J. Wind Eng. Ind. Aerodyn. 44, 2253–2264.

Dye, R.C.F., 1980. Comparison of full-scale and wind-tunnel model measurements of ground winds around a tower building. J. Wind Eng. Ind. Aerodyn. 6, 311–326.

First Sensor Ltd., 2019. LDE series-digital low differential pressure sensors.

Franke, J., Hellsten, A., Schlünzen, H., Carissimo, B., 2007. Best Practice Guideline for the CFD Simulation of Flows in the Urban Environment. Brussels, Belgium.

Franke, J., Hellsten, A., Schlunzen, K.H., Carissimo, B., 2011. The COST 732 Best Practice Guideline for CFD simulation of flows in the urban environment: a summary. Int. J. Environ. Pollut. 44, 419.

Gill Instruments Ltd., 2019. Wind Master 3-Axis Ultrasonic Anemometer.

Gökhan Ergin, F., Velte, C.M., 2017. Baseline measurements for testing of improved triple-sensor hot-wire anemometer probe in a momentum conserving turbulent round jet.

Hanafusa, T., Fujitani, T., Kobori, Y., Mitsuta, Y., 1982. A New Type Sonic Anemometer－Thermometer for Field Operation. Pap. Meteorol. Geophys. 33, 1–19.

Hanjalic, K., 2005. Will RANS Survive LES? A View of Perspectives. J. Fluids Eng. 127, 831.

Holmes, J., 2015. Wind loading of structures.

Hunt, J.C.R., Poulton, E.C., Mumford, J.C., 1976. The effects of wind on people; New criteria based on wind tunnel experiments. Build. Environ. 11, 15–28.

Immer, M.C., 2016. Time-resolved measurement and simulation of local scale turbulent urban flow. ETH-Zürich.

Irwin, H.P.A.H., 1981. A simple omnidirectional sensor for wind-tunnel studies of pedestrian-level winds. J. Wind Eng. Ind. Aerodyn. 7, 219–239.

Isyumov, N., Davenport, A.G., 1975. Comparison of full-scale and wind tunnel wind speed measurements in the commerce court plaza. J. Wind Eng. Ind. Aerodyn. 1, 201–212.

Isyumov, N., Davenport, A.G., 1976. The Ground Level Wind Environment in Built Up Areas. In: Proceedings of the Fourth International Conference on Wind Effects on Buildings and Structures. Cambridge University Press, U.K., pp. 403–422.

Jacob, J., Sagaut, P., 2018. Wind comfort assessment by means of large eddy simulation with lattice Boltzmann method in full scale city area. Build. Environ. 139, 110–124.

Jensen, K.D., 2004. Flow measurements. J. Brazilian Soc. Mech. Sci. Eng.

Jesson, M., Sterling, M., Letchford, C., Baker, C., 2015. Aerodynamic forces on the roofs of low-, mid- and high-rise buildings subject to transient winds. J. Wind Eng. Ind. Aerodyn. 143, 42–49.

Jordan, S.C., Johnson, T., Sterling, M., Baker, C.J., 2008. Evaluating and modelling the response of an individual to a sudden change in wind speed. Build. Environ. 43, 1521–1534.

Kaimal, J.C., 1979. Sonic anemometer measurement of atmospheric turbulence. 551–565.

Kamei, I., Maruta, E., 1979. Study on wind environmental problems caused around buildings in Japan. J. Wind Eng. Ind. Aerodyn. 4, 307–331.

Kuo, C.-Y., Tzeng, C.-T., Ho, M.-C., Lai, C.-M., 2015. Wind Tunnel Studies of a Pedestrian-Level Wind Environment in a Street Canyon between a High-Rise Building with a Podium and Low-Level Attached Houses. Energies 8, 10942–10957.

Lawson, T.V., Penwarden, A.D., 1976. The Effects of Wind on People in the Vicinity of Buildings. In: Proceedings of the Fourth International Conference on Wind Effects on Buildings and Structures. pp. 605–622.

Lawson, T. V., 1980. Wind effects on buildings, volume 1, design applications.

Leeds City Council, 2019. Draft Wind & Micro-climate Toolkit for Leeds - Leeds Local Plan - Supplementary Planning Document.

Lubitz, W.D., White, B.R., 2007. Wind-tunnel and field investigation of the effect of local wind direction on speed-up over hills. J. Wind Eng. Ind. Aerodyn. 95, 639–661.

Melbourne, W.H., 1978. Criteria for environmental wind conditions. J. Wind Eng. Ind. Aerodyn. 3, 241–249.

Miller, C.A., Davenport, A.G., 1998. Guidelines for the calculation of wind speed-ups in complex terrain. J. Wind Eng. Ind. Aerodyn. 74–76, 189–197.

Mittal, H., Sharma, A., Gairola, A., 2018. A review on the study of urban wind at the pedestrian level around buildings. J. Build. Eng.

Murakami, S., Deguchi, K., 1981. New criteria for wind effects on pedestrians. J. Wind Eng. Ind. Aerodyn. 7, 289–309.

NEN, 2006. Wind comfort and wind danger in the built environment, NEN 8100 (in Dutch) Dutch Standard.

Nicoud, F., Ducros, F., 1999. Subgrid-scale stress modelling based on the square of the velocity gradient tensor. Flow, Turbul. Combust. 62, 183–200.

Nosov, Lukin, Nosov, Torgaev, Bogushevich, 2019. Measurement of Atmospheric Turbulence Characteristics by the Ultrasonic Anemometers and the Calibration Processes. Atmosphere (Basel). 10, 460.

Penwarden, A.D., Grigg, P.F., Rayment, R., 1978. Measurements of wind drag on people standing in a wind tunnel. Build. Environ. 13, 75–84.

Peters, J., 1999. Air movements and human postural stability.

Roshko, A., 1993. Perspectives on bluff body aerodynamics. J. Wind Eng. Ind. Aerodyn. 49, 79–100.

Sagaut, P., 2006. Large eddy simulation for incompressible flows : an introduction. Springer-Verlag.

Sciacchitano, A., 2019. Uncertainty quantification in particle image velocimetry. Meas. Sci. Technol.

Shur, M.L., Spalart, P.R., Strelets, M.K., Travin, A.K., 2008. A hybrid RANS-LES approach with delayed-DES and wall-modelled LES capabilities. Int. J. Heat Fluid Flow 29, 1638–1649.

Soligo, M.J., Irwin, P.A., Williams, C.J., Schuyler, G.D., 1998. A comprehensive assessment of pedestrian comfort including thermal effects. J. Wind Eng. Ind. Aerodyn. 77–78, 753–766.

Spalart, P.R., Deck, S., Shur, M.L., Squires, K.D., Strelets, M.K., Travin, A., 2006. A new version of detached-eddy simulation, resistant to ambiguous grid densities. Theor. Comput. Fluid Dyn. 20, 181–195.

Stainback, P.C., Nagabushana, K.A., 1993. Review of hot-wire anemometry techniques and the range of their applicability for various flows. J. Fluids Eng. 1, 1–54.

Stathopoulos, T., 2006. Pedestrian level winds and outdoor human comfort. J. Wind Eng. Ind. Aerodyn. 94, 769–780.

Stathopoulos, T., Wu, H., 1995. Generic models for pedestrian-level winds in built-up regions. J. Wind Eng. Ind. Aerodyn. 54–55, 515–525.

Tabor, G.R., Baba-Ahmadi, M.H., 2010. Inlet conditions for large eddy simulation: A review. Comput. Fluids 39, 553–567.

The Guardian, 2017. Crashing waves and a collapsed roof: Storm Ophelia strikes - in pictures [WWW Document]. URL https://www.theguardian.com/uk-news/gallery/2017/oct/16/crashing-waves-and-cartwheels-storm-ophelia-strikes-in-pictures (accessed 11.27.19).

Tominaga, Y., Mochida, A., Yoshie, R., Kataoka, H., Nozu, T., Yoshikawa, M., Shirasawa, T., 2008. AIJ guidelines for practical applications of CFD to pedestrian wind environment around buildings. J. Wind Eng. Ind. Aerodyn. 96, 1749–1761.

Tsang, C.W., Kwok, K.C.S., Hitchcock, P.A., 2012. Wind tunnel study of pedestrian level wind environment around tall buildings: Effects of building dimensions, separation and podium. Build. Environ. 49, 167–181.

Tse, K.T., Weerasuriya, A.U., Zhang, X., Li, S., Kwok, K.C.S., 2017a. Pedestrian-level wind environment around isolated buildings under the influence of twisted wind flows. J. Wind Eng. Ind. Aerodyn. 162, 12–23.

Tse, K.T., Weerasuriya, A.U., Zhang, X., Li, S.W., Kwok, K.C.S., 2017b. Effects of twisted wind flows on wind conditions in passages between buildings. J. Wind Eng. Ind. Aerodyn. 167, 87–100.

TurbulentFlow Instrumentation Inc., 2015. Getting Started - Series 100 Cobra Probe.

Uematsu, Y., Yamada, M., Higashiyama, H., Orimo, T., 1992. Effects of the corner shape of high-rise buildings on the pedestrian-level wind environment with consideration for mean and fluctuating wind speeds. J. Wind Eng. Ind. Aerodyn. 44, 2289–2300.

Visser, G.T., Cleijne, J.W., 1994. Wind comfort predictions by wind tunnel tests: comparison with full-scale data. J. Wind Eng. Ind. Aerodyn. 52, 385–402.

Wieringa, J., 1986. Roughness-dependent geographical interpolation of surface wind speed averages. Q. J. R. Meteorol. Soc. 112, 867–889.

Williams, C.D., Wardlaw, R.L., 1992. Determination of the pedestrian wind environment in the city of Ottawa using wind tunnel and field measurements. J. Wind Eng. Ind. Aerodyn. 41, 255–266.

Wu, H., Stathopoulos, T., 1993. Wind-Tunnel Techniques for Assessment of Pedestrian-Level Winds. J. Eng. Mech. 119, 1920–1936.

Wu, H., Stathopoulos, T., 1994. Further experiments on Irwin's surface wind sensor. J. Wind Eng. Ind. Aerodyn. 53, 441–452.

Wu, H., Stathopoulos, T., 1997. Application of Infrared Thermography for Pedestrian Wind Evaluation. J. Eng. Mech. 123, 978–985.

Wyngaard, J.C., Zhang, S.-F., Wyngaard, J.C., Zhang, S.-F., 1985. Transducer-Shadow Effects on Turbulence Spectra Measured by Sonic Anemometers. http://dx.doi.org/10.1175/1520-0426(1985)002<0548:TSEOTS>2.0.CO;2.

YinMun, H., Ikegaya, N., bin Salim, S.A.Z.S., Hagishima, A., Yusri, Y., 2019. Pedestrian Wind Distribution Within an Urban University City Campus using Wind Tunnel Test. Int. J. Recent Technol. Eng. 8, 373–382.

Yoshie, R., Mochida, A., Tominaga, Y., Kataoka, H., Harimoto, K., Nozu, T., Shirasawa, T., 2007. Cooperative project for CFD prediction of pedestrian wind environment in the Architectural Institute of Japan. J. Wind Eng. Ind. Aerodyn. 95, 1551–1578.

Zhang, X., Tse, K.T., Weerasuriya, A.U., Kwok, K.C.S., Niu, J., Lin, Z., Mak, C.M., 2018. Pedestrian-level wind conditions in the space underneath lift-up buildings. J. Wind Eng. Ind. Aerodyn. 179, 58–69.

Zheng, C., Li, Y., Wu, Y., 2016. Pedestrian-level wind environment on outdoor platforms of a thousand-meter-scale megatall building: Sub-configuration experiment and wind comfort assessment. Build. Environ. 106, 313–326.